Materials and Design 173 (2019) 107762

Contents lists available at ScienceDirect

Materials and Design

journal homepage: www.elsevier.com/locate/matdes

A review of experimental approaches to fracture toughness evaluation at the micro-scale

J. Ast [a], M. Ghidelli [b,c], K. Durst [d], M. Göken [e], M. Sebastiani [f], A.M. Korsunsky [g,*]

[a] EMPA, Swiss Federal Laboratories for Materials Science and Technology, Feuerwerkerstrasse 39, 3602 Thun, Switzerland
[b] Micro- and Nanostructured Materials Laboratory, Politecnico di Milano, Piazza Leonardo da Vinci 32, 20133 Milano, MI, Italy
[c] Structure and Nano/-Micromechanics of Materials, Max-Planck-Institut für Eisenforschung GmbH, Max-Planck-straße 1, 40237 Düsseldorf, Germany
[d] Physical Metallurgy, Technical University of Darmstadt, Alarich-Weiss-Straße 2, 64287 Darmstadt, Germany
[e] General Materials Properties, FAU Erlangen-Nürnberg, Martensstraße 5, 91058 Erlangen, Germany
[f] Engineering Department, Universitá degli studi Roma Tre, Via della Vasca Navale 79, Rome, Italy
[g] Multi-Beam Laboratory for Engineering Microscopy, Department of Engineering Science, University of Oxford, Parks Rd, Oxford OX1 3PJ, UK

HIGHLIGHTS

- Review of toughness evaluation at the micro- to nano-scale
- Fundamentals and applications of micro-pillar splitting testing
- Fundamentals and applications of micro-cantilever testing
- Overview of achievements, challenges and opportunities

GRAPHICAL ABSTRACT

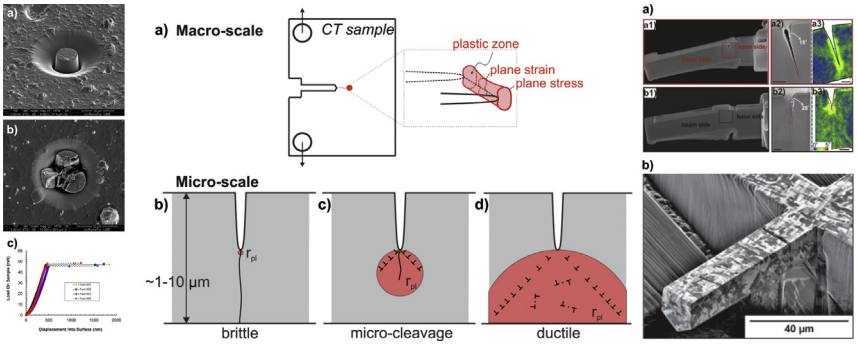

ARTICLE INFO

Article history:
Received 31 October 2018
Received in revised form 10 March 2019
Accepted 23 March 2019
Available online 25 March 2019

Keywords:
Fracture toughness
Micro-scale
Focused ion beam milling
Material characterisation
Micro-mechanics

ABSTRACT

The discipline of fracture mechanics was born almost a century ago through the pioneering work of A.A. Griffith, and saw particularly rapid growth in the second half of 20th century when it became an indispensable tool in the development of advanced transportation, civil construction, and energy systems. Forty years ago, *Materials & Design* published a series of papers devoted to the state-of-the-art in the field of Fracture Mechanics. The present review reflects the lasting legacy and surviving importance of this theme: it is associated with the Virtual Special Issue on nanoscale materials testing and characterisation, and focuses on the modern experimental approaches to fine scale fracture toughness evaluation, with particular emphasis on micro-cantilever bending and micro-pillar splitting. The fundamental aspects of these approaches are overviewed, and their application to a range of systems is described. Implications for further development of these methods are discussed.

© 2019 The Authors. Published by Elsevier Ltd. This is an open access article under the CC BY-NC-ND license (http://creativecommons.org/licenses/by-nc-nd/4.0/).

In 1978–79, a series of seminal papers entitled "*An introduction to fracture mechanics for engineers*" was published by Rod Smith in v.1 of this journal (then known as *International Journal of Materials in Engineering Applications*).In 2018, as *Materials & Design* celebrated its 40th anniversary, the journal is going from strength to strength,

* Corresponding author.
E-mail address: alexander.korsunsky@eng.ox.ac.uk (A.M. Korsunsky).

https://doi.org/10.1016/j.matdes.2019.107762
0264-1275/© 2019 The Authors. Published by Elsevier Ltd. This is an open access article under the CC BY-NC-ND license (http://creativecommons.org/licenses/by-nc-nd/4.0/).

increasing its profile and impact in the ever-broader field of materials engineering, whilst retaining its strong focus on mechanical phenomena and characterisation techniques.It is therefore appropriate and timely to revisit the important topic of toughness testing in this overview, to present the modern developments and frontier approaches at increasingly fine scales.

1. General introduction

The concept of toughness as the measure of resistance to fracture emerged almost a century ago through the pioneering work of Griffith [1], who identified the crucial role of the energy release rate in determining the structural integrity of brittle materials. Griffith's work was motivated by two earlier developments: the elastic solution for the stress field around an elliptical void in an infinite plane by Inglis [2], and the development of thermodynamics by Josiah Willard Gibbs [3] that led to the derivation of the Gibbs-Thomson equation, e.g. [4]. Gibbs' thermodynamics not only allowed rational description of the coexistence and transformation of phases, but also the identification of the critical nucleus size for new phase formation by nucleation and growth. This follows from the analysis of total Gibbs free energy comprising the volume and surface terms:

$$\Delta G = \Delta g^p \cdot \frac{4}{3}\pi r^3 + \gamma_s \cdot 4\pi r^2, \tag{1}$$

where ΔG stands for the total change in the Gibbs free energy of the system, Δg^p is the specific (per unit volume) Gibbs free energy change due to the phase transformation, γ_s is the specific (per unit area) energy associated with the new interfaces being created, and r denotes the radius of a spherical nucleus. Differentiation of this expression leads to:

$$\frac{\partial \Delta G}{\partial r} = \Delta g^p \cdot 4\pi r^2 + \gamma_s \cdot 8\pi r. \tag{2}$$

Since the phase transformation is associated with the reduction in energy, Δg^p is negative, and the above expression becomes zero at the critical nucleus size,

$$r^* = \frac{2\gamma_s}{|\Delta g^p|}, \tag{3}$$

which corresponds to a maximum of ΔG. Therefore, at $r < r^*$ it is thermodynamically favourable for the system to reduce energy by dissolving the nucleus, whilst for $r > r^*$ the nucleus will grow.

The key element of the above derivation is the occurrence within the expression for the free energy of a sum of two terms, each displaying a different dependence on the linear dimension of the nucleus: quadratic for surface energy, and cubic for volume. It is the combination of these terms that leads to the emergence of a length scale that is related to the critical nucleus size.

Griffith's approach followed the same logic in application to the process of crack extension. He observed that a body containing a crack and subjected to external or residual stress acts like a spring that stores elastic strain energy. In order for the crack to grow, the volumetric elastic strain energy must be released, and then consumed to create fresh fracture surfaces. Using the usual notation E for Young's modulus, and a for the length (or half-length) of a planar crack, the total energy change per unit width of the sample was written as:

$$\frac{\Delta G}{b} = -\frac{\sigma^2}{2E} \cdot \pi a^2 + \gamma_s \cdot 2a, \tag{4}$$

where γ_s retains the meaning of surface energy per unit area. The derivative becomes:

$$\frac{1}{b}\frac{\partial \Delta G}{\partial a} = -\frac{\sigma^2}{2E} \cdot 2\pi a + \gamma_s \cdot 2, \tag{5}$$

and it is found that the critical crack length must satisfy the following Griffith criterion:

$$\sigma^2 \pi a^* = 2\gamma_s E. \tag{6}$$

Griffith further re-wrote this relationship as

$$\frac{\sigma^2 \pi a^*}{E} = G_C, \tag{7}$$

and introduced the term 'critical energy release rate' and 'material toughness', which for the elastic-brittle case considered above is given by $G_C = 2\gamma_s$, whilst in the more general situation must include contributions from plastic flow, phase transformation, etc.

Further work by Irwin [5] and others ushered in the alternative measure known as *fracture toughness*. Unlike Griffith, Irwin placed the focus on the stress-strain distribution in the vicinity of the crack tip, and defining its multiplicative measure, the stress intensity factor. For example, for Mode I, in the local polar coordinates associated with the crack tip, the stress in the crack opening direction is given by:

$$\sigma_{yy}(r,\theta) = \frac{K_I}{\sqrt{2\pi r}} \cos\theta/2(1 + \sin\theta/2 \sin 3\theta/2). \tag{8}$$

It is clear that the stress is singular, i.e. tends to infinity as $r \to 0$. Nevertheless, K_I provides a quantitative measure of the severity of this phenomenon, and can be used to assess the propensity of a crack to grow. In fact, a critical value of this parameter, K_{IC}, can be assumed a material property, and is called 'fracture toughness'.

Furthermore, a direct relationship was established between the two measures of resistance to cracking, toughness G_c and fracture toughness K_{Ic}, which encapsulates the above formulae in the case of plane stress state:

$$\sigma^2 \pi a^* = G_c E = K_{Ic}^2. \tag{9}$$

In practice, for complex sample shapes, corrective geometric scaling factor Y needs to be introduced.

The central statement of Linear Elastic Fracture Mechanics (LEFM) is the declaration that crack extension occurs when the stress intensity factor K_I, expressed in terms of the stress σ and crack (half-)length a, reaches the critical value K_{Ic}:

$$K_I = Y\sigma\sqrt{\pi a} = K_{Ic}. \tag{10}$$

This criterion connects the material property, problem geometry, and loading conditions. It is therefore worth noting that this critical condition can arise either due to increasing applied load, or extension of the crack, or the reduction of material fracture toughness.

Further complexities arise when considering the fracture process as soon as the material response is no longer elastic-brittle, but includes plastic deformation in the vicinity of the crack tip. This clearly alters the stress field, so that elastic equations such as Eq. (8) no longer apply. Whilst LEFM framework can be adapted by introducing approximations, it is clear that the energy-based Griffith approach possesses greater generality. Indeed, in the discipline of elasto-plastic fracture mechanics (EPFM) it has been generalised by Hutchinson [6], and Rice and Rosengren [7] in the form of J-Integral that applies to non-linearly elastic materials, as well as many other advances that are referred to and drawn upon in the present overview.

The classical definition of stress (as well as that for strain) as force per area, relies on the consideration of a reference cross-section, or

volume. Therefore, a dependence on scale is inherent in the very definition of stress. It is an evident corollary that fractures toughness, e.g. as formulated on the basis of stress distribution analysis, must similarly be a scale-dependent quantity. Therefore, both G_c and K_{Ic} must show a dependence on the scale of consideration. This does not simply concern different spatial resolution of measurements, but rather the scale-dependent change of the very physical quantities one wishes to determine. The implication here is that in the experimental toughness evaluation, the scale dependence, or the fracture toughness size effect, are inherent phenomena that cannot be overcome merely by the optimisation of measurement techniques. In order to provide appropriate input into deformation and fracture analysis at the chosen scale, toughness determination must be carried out using specimens and tests of corresponding dimensions.

Toughness (and fracture toughness) are coarse-graining properties, in that they provide a measure perceived at certain dimensional scale of the energy dissipation required for crack advance across the sample. This depends on the sum total (integral) taken over the structure and defects present within the material at finer scales. This explains why the presence of fine scale voids or micro-cracks reduces the apparent toughness perceived at the next level of consideration, whilst ductile inclusions or deformation-induced phase transformation ahead of the crack tip (such as in rubber-toughened polymers or in transformation-toughened zirconia) increase the apparent crack propagation resistance of the material.

The above analysis gives the imperative for fine scale toughness testing, through the preparation of miniature specimens containing micro- to nano-scale cracks, the use of ultra-low load, high displacement resolution mechanical testing devices, high resolution imaging, and validation against appropriate models. Toughness size effects arise in single crystal, polycrystalline and amorphous materials due to the interaction between characteristic dimensions, of which the critical crack length that arises in Griffith analysis is one. A whole range of other characteristic length scales can be identified. The most obvious is associated with plastic zone radius: when this becomes comparable with the crack length, 'interaction' is observed, in the form of the alteration of apparent toughness. Other significant length scales are the outer sample dimensions, grain size, distance between pre-existing dislocations and the associated strain gradients, etc. In this respect, toughness analysis at the micro-scale is 'rich', i.e. depends strongly on the specific sample geometry and micro-/nano-structure.

In the present review article, we summarize the approaches proposed and applied to tackle the challenges outlined above, with particular emphasis on micro-cantilever and micro-pillar test configurations. We illustrate by example the insights obtained using them, and discuss the implications of these findings for structural design against failure across the scales.

2. Classical indentation-based methods

Sharp indentation-based models for fracture toughness evaluation rely on the direct measurement of the radial cracks originating at the edge of a Vickers (or Berkovich) indentation mark, according to the scheme reported in Fig. 1. Maybe reduce dimensions of image in the final version. The original Lawn-Evans-Marshall (LEM) [8–11] approach leads to the following very well-known equation:

$$K_c = \alpha \cdot \sqrt{\frac{E}{H}} \cdot \frac{P_{max}}{c^{3/2}}, \tag{11}$$

where c is the average crack length, H the hardness of the material and P_{max} the maximum load during indentation. The value of the coefficient α has been experimentally quantified for a series of brittle (bulk) materials and found to be ~0.016 for the Vickers 4-sided pyramidal indenter. Further studies have identified specific coefficients for different indenter geometries [12].

Since its original development, several studies have shown that the application of the original LEM model was appropriate only for the case of brittle bulk ceramics, where the dimensions of the radial cracks are usually much larger than the size of the indentation mark, the accompanying so-called 'half-penny' crack geometry. In cases when crack shape differs significantly from the half-penny reference, the application of the LEM model could lead to wrong (or at least inaccurate) estimations of fracture toughness.

Several other models have been proposed in the last few decades [13–16], to take different possible crack geometries and material property combinations into account. In particular, the choice of the proper model for determining the indentation fracture toughness depends on the type of the geometry of crack systems, e.g., median, radial, half-penny, cone, or lateral cracks (see Fig. 1), and the geometry of the pyramidal indenter. More recent research efforts have used cohesive-zone finite element modelling (CZ-FEM) to simulate such effects as inelastic densification effects, plastic deformation, crack nucleation and growth during sharp indentation. Such studies [17–19] have shown that the coefficient α from the LEM model actually depends considerably on the ratio E/H (or, equivalently, E/σ_y, where σ_y is the yield stress), Poisson's ratio, and the indenter geometry. In particular, the median crack geometry is predominant for brittle materials with E/σ_y ~10, whereas the radial (often referred to as Palmqvist) geometry is the most likely one for metallic-like materials (E/σ_y ~ 100). Detailed functions for the coefficient α for a wide range of material properties and indenter angles can be found in references [17, 18], which can be effectively used for a proper use of indentation based methods for evaluation of fracture toughness.

However, the choice of the most proper model to use can be extremely challenging in practical cases, because of (a) possible uncertainties in the determination of E/σ_y ratio and (b) the presence of residual stress in the material. The latter case is crucial for thin films and coatings, where the presence of a compressive residual stress could make it impossible to generate radial cracks after sharp indentation testing. To overcome the evident limitations of the classical indentation-based methods for fracture toughness assessment at the micron-scale, new experimental methodologies have been recently proposed. Such methods normally make use of a nanoindenter to test micro-scale specimens of various geometries, produced by focused ion beam (FIB) machining [20–22]. Specimen geometries can include pillars (shown below), membranes [23–25], micro-tensile specimens [26], double clamped beams [27,28], and single (shown below) and double [29,30] cantilever beams.

In the following chapters, we will review the two most popular experimental approaches for fracture toughness determination at the micro-scale:

- The pillar splitting method, which is based on a sharp nanoindentation of a micro-pillar. This technique is particularly useful for testing of thin ceramic films.
- The micro-cantilever method, which is very versatile and an important tool for the analysis of fracture mechanisms in brittle and semi-brittle materials.

3. Micro-pillar splitting

3.1. Introduction

The *micro-pillar splitting* method for fine scale fracture toughness determination was developed by Sebastiani et al. [31] as a complementary small-scale technique for the determination of K_c. The method is based on the use of a sharp indenter to indent micro-pillars (fabricated by FIB-milling or otherwise) with an aspect ratio (height/diameter) larger than 1 (Fig. 2). After the initial setting in trend in the load-depth curve, following the usual parabolic Kick's law for sharp indentation, in

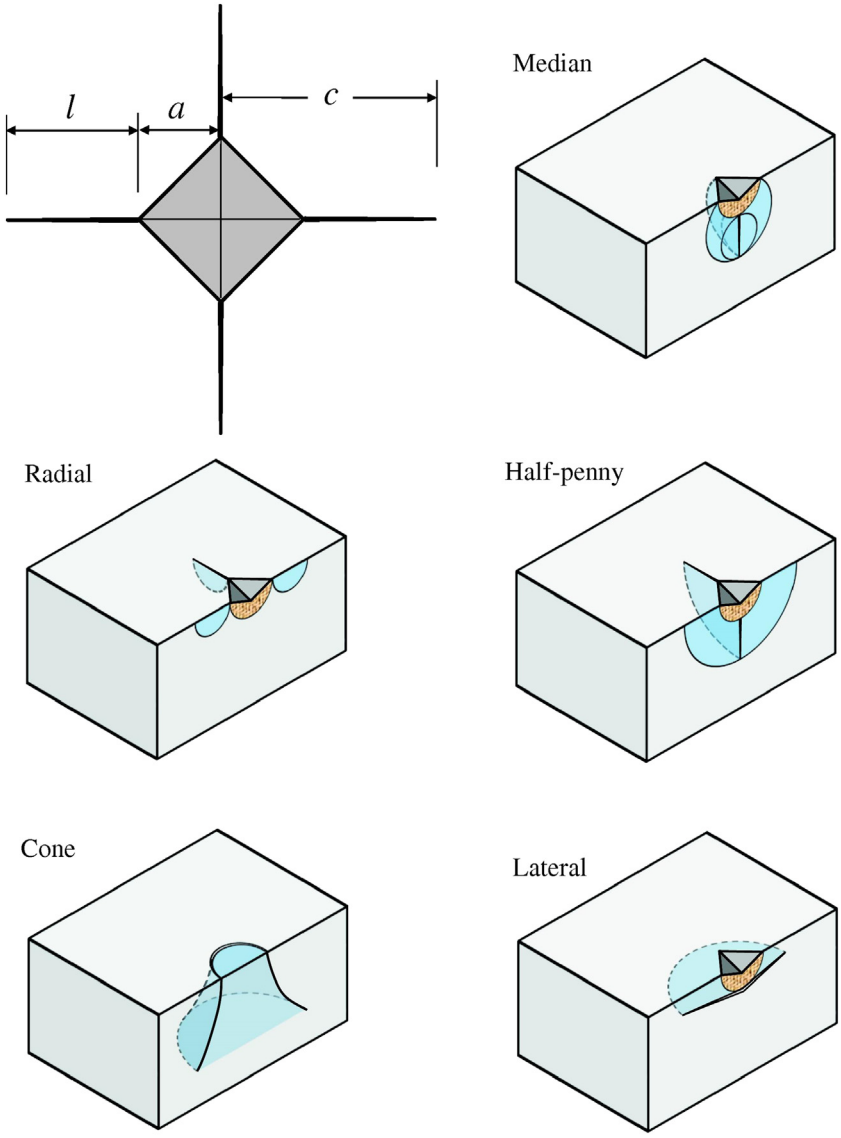

Fig. 1. Example of possible crack geometries under sharp indentation loading. Reproduced with permission from references [17].

sufficiently brittle materials, a crack nucleates underneath the indenter. Once a critical load is reached, the crack extends (pops) out to the pillar surface (Figs. 2b and 3a,b).

Under these testing conditions, K_c can be estimated on the basis of the critical splitting load P_c, i.e. the load at which a displacement burst is detected in the load-displacement curve (Fig. 2c), the pillar radius R, and a calibration coefficient γ, through the relation:

$$K_c = \gamma \frac{P_c}{R^{3/2}} \tag{12}$$

Modelling pillar indentation cracking by CZ-FEM showed that the load drop occurred consistently at a unique value of $P/(K_c R^{3/2})$ for given material [31], thus confirming the validity of Eq. (12) for extracting K_c. More details on the derivation and validation of Eq. (12) are reported in [32]. CZ-FEM was also used to determine the coefficient γ, taking into account crack propagation within the pillar, the indenter geometry, as well as the material properties, namely, Poisson's ratio ν, and the E/H ratio.

Micro-pillar splitting testing combines the advantages of the standard indentation cracking technique with the ease of application and the high spatial resolution. The measurement of crack length is not required, and residual stresses do not affect the result, because they are completely released by the FIB milling process [31,32]. Here, it is worth mentioning that residual stress can induce cantilever bending [33], and thus may affect the outcome of tests involving that geometry. Furthermore, detailed knowledge of the crack shape and length is a requirement for cantilever techniques (see Section 4). In addition, Best et al. [34] suggested that compared to cantilever-based techniques, the effects of ion damage in micro-pillar splitting are significantly reduced (although not completely avoided), since crack nucleation and growth before instability occur in the core of the pillar, where FIB damage is rather low compared to the micro-pillar side surface (see Section 5). Lastly, it is worth noting that large pillar arrays can be easily milled to provide significant statistical basis for collecting information on K_c, whilst the complexity of cantilever bending technique often limits the number of available specimens, resulting in a poor statistical analysis. For these reasons, micro-pillar splitting has been recently adopted and applied to different classes of materials, such as bulk silicon (100), ceramic thin films (TiN, CrN), and composite multi-layers (CrAlN/Si_3N_4) [31,32,35,36]. Moreover, this method has also been successfully applied for the estimation of K_c for Al-substituted $Li_7La_3Zr_2O_{12}$ [37] and $Li_xMn_2O_4$ oxides used for battery cathode applications [38,39]. These studies will be reviewed in more detail in Section 3.5.

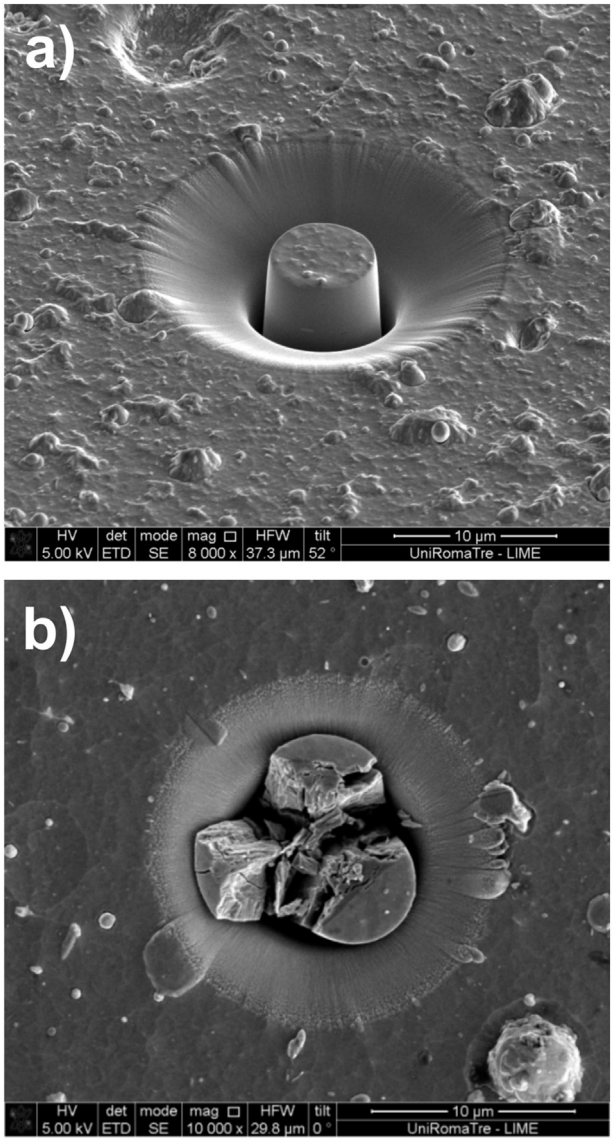

Fig. 2. (a) Example of a CrAlN/Si_3N_4 pillar before splitting. (b) Example of a CrN pillar after splitting. (c) Load-displacement curves for CrN pillars, highlighting the critical load (P_c) corresponding to the crack 'popping out' to the side surface, and pillar splitting [31]. Reproduced with permission [31].

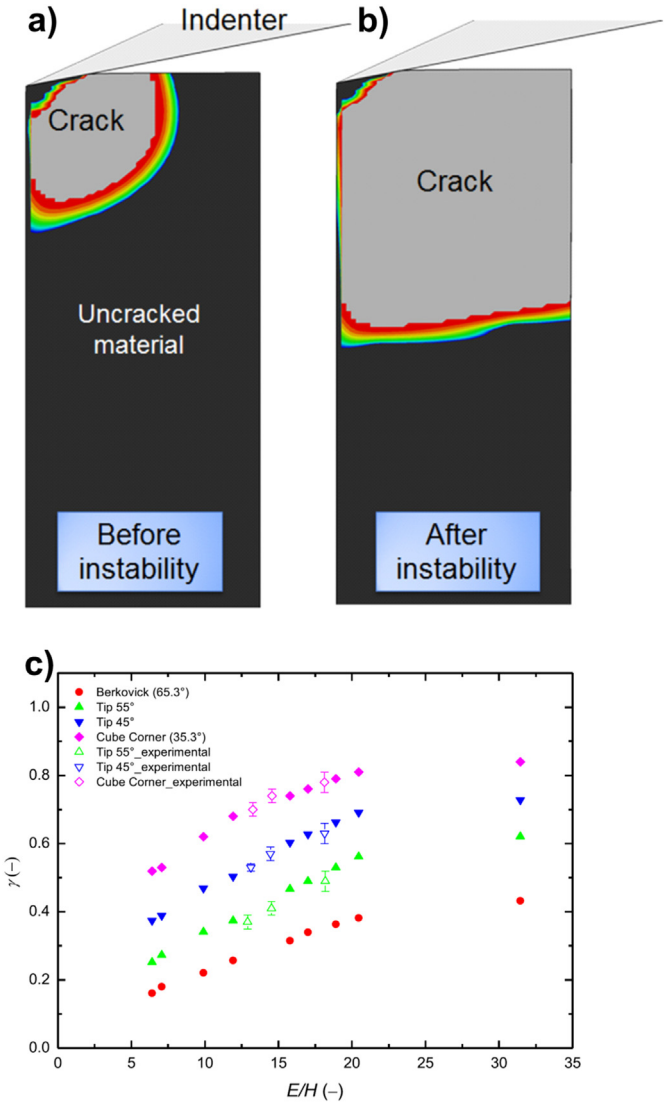

Fig. 3. (a, b) Crack geometries in a representative pillar splitting test just before and just after the instability load, respectively [32]. (c) γ (gamma) coefficient as a function of E/H for different tip geometries. The solid and empty symbols represent, respectively, FEM simulations and experimental data [35]. Reproduced with permission from references [32] and [35], respectively.

3.2. Method development and calibration by CZ-FEM

In the previous section, we reviewed the basics for the extraction of fracture toughness using the micro-pillar splitting technique. Although the application of this technique may appear to be rather easy, the quantitative interpretation of the micro-pillar splitting method relies on the use of CZ-FEM to extract the dimensionless coefficient γ which relates the fracture toughness K_c to the splitting load P_c and the pillar radius R, Eq. (12). In addition, it is important to note that γ is a material and geometry-dependent quantity, i.e., it varies as a function of E/H and Poisson's ratio, as well as with the indenter geometry [31]. Therefore, setting the proper γ coefficient for a given experiment (indenter geometry and sample material) relies on the knowledge of indenter-sample interaction and mechanical properties. Inaccuracies in the quantitative fracture toughness determination may also arise from the CZ-FEM procedures, where the models adopted typically assume ideal geometries for both the indenter and micro-pillar. However, experience shows that rather accurate results can be obtained by using pillars with low taper angle and sharp indenters (with small tip radius).

The identification of coefficient γ was initially carried out for a limited set of intrinsically brittle materials (including TiN, CrN and CrAlN/Si_3N_4), for a Berkovich indenter geometry (with the face angle of 65.3°), and a constant Poisson's ratio equal to 0.25. FEM simulations were carried out using ABAQUS software (v6) for perfectly cylindrical pillars of isotropic material with an elastic-perfectly plastic behaviour (no work hardening). Cohesive elements were installed along each of the indenter edges on a plane perpendicular to the free sample surface. With this geometry, the crack growth is dictated by material properties, loading conditions, and pillar geometry, but it was constrained to remain within the defined crack plane according to the cohesive element definition. A MAXS criterion (maximum stress) was used for the onset of debonding, and a fracture energy criterion was used for crack nucleation [31,32]. It is worth mentioning that the adopted input parameters for CZ-FEM could be an additional source of uncertainty for the calculated gamma coefficient. This issue surely deserves a more comprehensive parametric FEM study in the future.

Fig. 3 reports the crack geometries predicted by the finite element simulations just before (a) and just after (b) the critical instability load P_c, for the same material. It can be observed that the crack propagates along the cohesive element planes, whilst a load drop is observed once the crack reaches the pillar edge [32]. After validation of this methodology, CZ-FEM has been further improved taking into account the effect of the substrate, whilst investigating ceramic materials with different E/H, but constant Poisson's ratio equal to 0.25. For different substrates (with E varying from 2 up to 200 GPa), it has been found that the critical load is very weakly dependent on the substrate elastic properties [32]. This enables the application of pillar splitting on thin films deposited on more compliant substrates.

Fig. 3c includes additional FE results for values of γ in the E/H range from 5 to 31, and different indenter geometries, including a Berkovich tip (65.3°) and cube corner (35.3°) [35]. The results for the Berkovich tip (red dots) are the same as those in [32], in which γ increases from 0.145 ($E/H = 7.0$) up to 0.4 ($E/H = 31$). A similar trend is observed for other indenter geometries, with a shift to higher γ values for sharper indenters. These results are in good agreement with the analogous trend reported in Ref. [17] for the function $f(H)$ that relates K_c to the applied load and crack length during standard nanoindentation experiments using the LEM model. The γ coefficient values calculated for indenter geometries with inter-face angles of 55°, 45°, and 35.3°(cube corner) were verified assuming the "true" constant fracture toughness obtained using the Berkovich indenter, for which the γ coefficient had already been validated [35]. In Fig. 3c, it can be observed that the γ coefficient estimated with this method (open symbols) is in good agreement with the trend of γ obtained from FEM calculations with different indenter geometries (closed symbols).

To expand further the application range of the micro-pillar splitting method, the effect of Poisson's ratio was investigated for different E/H ratios for Berkovich indenter specifically [35]. Poisson's ratio was varied from 0.20 to 0.30 for the E/H interval between 7 and 23, whilst it has been varied from 0 up to 0.40 for E/H equal to 31. A weaker dependence of γ on Poisson's ratio was reported for the E/H interval 7–23, in which the variation of γ was ± 0.03, whereas a larger effect was found for E/H equal to 31, for which the variability of γ was around ± 0.05 with respect to the estimated value considering $\nu = 0.25$. All results for the values of γ are tabulated in [35].

3.3. Effects of indenter geometry and positioning accuracy

In this section, we review the effect of the indenter angle and the positioning accuracy on the estimates of fracture toughness by micro-pillar splitting. Along with expanding the range of materials that can be investigated, this aspect provides information about the accuracy of K_c estimate as a function of distance of indent from the pillar center.

The effect of the indenter angle has been studied in [35], in which different indenters were investigated with angles ranging from 65.3° (Berkovich) to 35.3° (cube corner). Fig. 4A shows load-depth curves for Si (100) pillars with different indenter geometries, along with a load-depth curve for Berkovich indentation in bulk Si. The splitting load varied as a function of the indenter geometry from 16.14 mN for the Berkovich tip down to 5.11 mN for the sharper cube-corner indenter. Furthermore, the load-depth curves obtained for bulk Si (100) and for the micro-pillar using the Berkovich indenter were found to be very similar, showing only a slight divergence near the splitting load. Similar trends were observed for TiN and CrN thin films, for which residual stresses were released during micro-pillar fabrication [31,32].

Fig. 4B shows the splitting load as a function of the indenter angle for the three materials. In general, for a given diameter, the splitting load increases linearly for larger indenter angles. The sharper indenter provokes a reduction in the splitting load because of the large stress intensification. More interestingly, the slope of the splitting load as function of the indenter angle is found to be almost independent of the pillar diameter, respectively, 5 μm for TiN and Si and 3 μm for CrN. As a result, 5 μm diameter TiN pillars (which were investigated in [35]) show a splitting load which is linearly shifted towards larger values with increasing pillar diameter according to Eq. (12).

The extraction of K_c for different indenter geometries was done using the splitting loads P_c in Fig. 4B and the γ coefficients reported in Fig. 3c for different indenter geometries. In Ref. [35] it was found that the value of K_c is independent of the indenter angle. This represents a preliminary validation of the CZ-FEM, whilst suggesting that γ is not too sensitive to frictional effects, which often become more pronounced for sharper indenters. Thus, cube-corner indenters, which induce

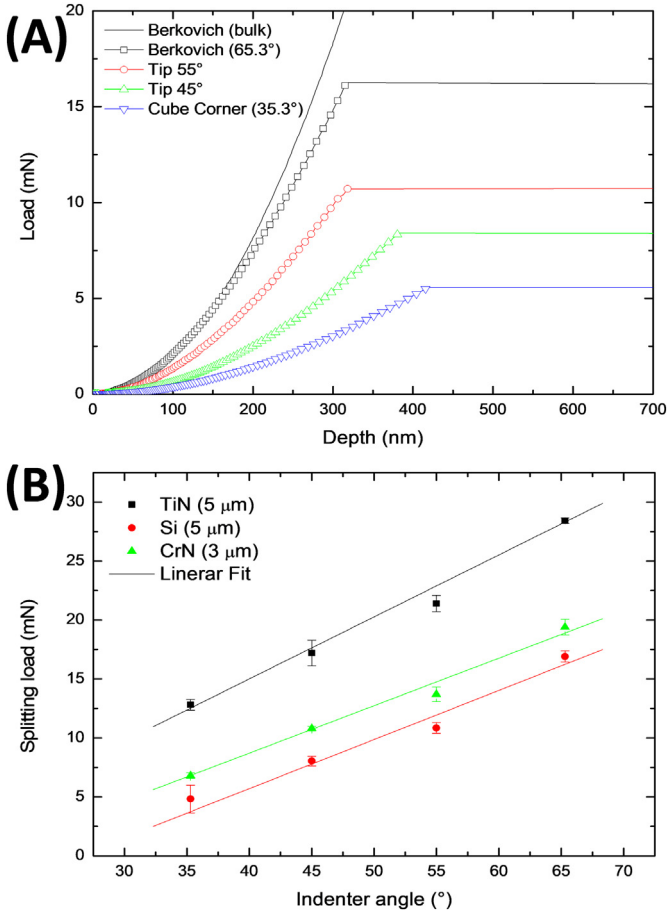

Fig. 4. (A) Experimental results for pillar splitting of Si (100). The effects of the indenter geometry on the splitting load are highlighted. (B) Average splitting load as a function of the indenter angle for each of the three materials [35]. Reproduced with permission from reference [35].

cracking at much lower loads than Berkovich indenters, can be used effectively in pillar splitting experiments.

One of the advantages of using sharper indenters is the possibility to expand the pillar splitting method to materials which exhibit higher K_c. Smaller micro-pillar radii would have been required in order to achieve lower splitting loads, according to Eq. (12). Therefore, the use of a sharper indenter reduces the minimum required pillar diameter to obtain crack initiation, which is possibly of great interest for brittle intermetallic materials and high-temperature K_c assessment as discussed in sections 3.4 and 3.5.

A significant advantage of the micro-pillar splitting with respect to other small-scale techniques is the possibility to carry out ex situ nanoindentation testing [31,32]. This improves the applicability of this technique for industrial needs aiming to extract K_c for bulk materials and coatings. However, to perform accurate micro-pillar splitting testing, the indent must be placed as precisely as possible at the micro-pillar center [31,32]. This enables crack propagation imposed by the indenter geometry, and ensures that correct value of K_c is obtained from the γ coefficient extracted from CZ-FEM. Inaccuracy in the position can arise also during in situ (SEM) testing which allows very accurate positioning of the indenter above the pillar in one direction (X-axis, across SEM beam), but reduced accuracy in the depth (Y-axis, along SEM beam) due to sample tilt.

For these reasons, Lauener et al. [36] investigated the effect of the indent positioning on the fracture toughness value extracted by micro-pillar splitting. Fig. 5 reports apparent K_c values as a function of indent distance from micro-pillar center. Two different indenter geometries were used for this experiment. The investigation was performed on pillars with a diameter of 5 μm, using two different cube corner indenters with tip radii of ~500 and ~200 nm. For both indenters the evaluated fracture toughness remained unchanged for indents offset from the micro-pillar center by distances up to 350 nm, corresponding to up to 14% of the pillar radius. However, the sharper indenter caused the load instability at lower stress intensity, as might be expected. At larger offsets, the apparent K_c values decreased from 0.8 down to 0.2 MPa $m^{1/2}$ as the edge of the pillar was approached. This trend can be explained considering that for large off-center indenter positioning (i.e. >0.2 fraction of pillar radius), Eq. (12) is no longer valid, since the critical load P_c is reduced. The propagation distance for one of the cracks formed from indenter facet edge to the pillar side surface is reduced, whilst for the other two these are increased [36]. In the same study, the authors also showed that the critical load for instability was practically insensitive to the indenter tip speed within the range 2–50 nm/s.

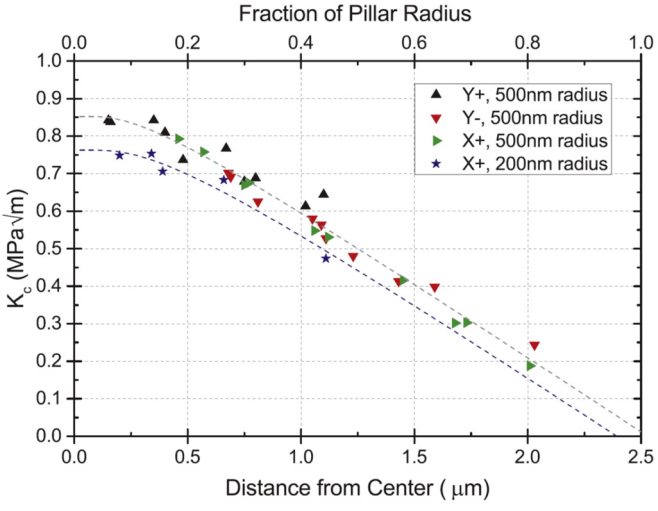

Fig. 5. Apparent fracture toughness as a function of distance to the center of the pillar with the offset orientation direction and the indenter tip radius noted [36]. Reproduced with permission from reference [36].

3.4. Practical guidelines for method application

The use of pillar splitting method to extract K_c has so far been adopted for ceramic materials, for which a crack can nucleate and propagate easily upon indentation. As a matter of fact, the necessary condition for the application of Eq. (12) is that the critical load for unstable crack propagation is reached and clearly identified in the experimental load-displacement curve. The method has been successfully applied to several nitrides (i.e. CrN, TiN, CrAlN/Si_3N_4), oxides, single-crystal Si, and selected materials from other classes for which brittle mechanical behaviour has been reported (Fig. 6).

The method has also been attempted for metallic materials for the case of bulk metallic glass (BMG) [32]. However, neither crack nucleation nor unstable propagation was observed. This result has been confirmed for a range of pillar diameters between 2 μm and 15 μm, all with a fixed aspect ratio equal to 1.0. The deformation of BMG samples occurred mostly by the propagation of discrete shear bands that were visible as a series of serrations in the load–displacement curve. BMGs can exhibit large values of fracture toughness (>50 MPa $m^{1/2}$), so that in order to nucleate a crack by pillar splitting, larger loads or the use of large pillar diameters is required, in accordance with Eq. (12).

A more detailed study of the conditions for crack nucleation and propagation leads to the establishment of a simple equation for the minimum diameter of micro-pillar required to achieve splitting during testing:

$$d = \sqrt{2\chi} \cdot \frac{K_{Ic}^2}{H^2}, \tag{13}$$

where K_c is expressed in MPa $m^{1/2}$, H in GPa, and d in μm. Here χ is a coefficient that depends on the indenter geometry (equal to $2.2 \cdot 10^4$ for a Vickers indenter, with linearly decreasing values for sharper indenter angles [35]). According to the same reference, the χ coefficient becomes equal to $1.0 \cdot 10^4$ for a cube-corner indenter, thus allowing for the estimation of the critical pillar diameter also for the case of cube-corner. One may assume a maximum possible micro-pillar diameter of 100 μm as a limit that could be achieved using modern FIB systems, including plasma systems. It then becomes clear from Eq. (13) that in order to have unstable splitting by a cube-corner indenter the K_c/H ratio should be lower than 0.8 (which roughly corresponds to $K_c/HV \sim 0.008$, if Vickers hardness HV is measured in kgf/mm^2).

Fig. 7 is a chart for commercial engineering bulk materials showing possible materials classes and families for which toughness can be evaluated by indentation splitting with the maximum micro-pillar diameter

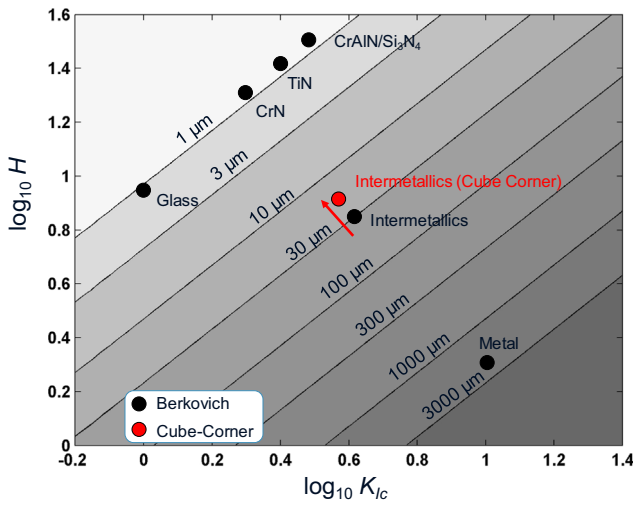

Fig. 6. A practical selection map showing that this method could be reliably applied to ceramics and some intermetallics [32]. Reproduced with permission from reference [32].

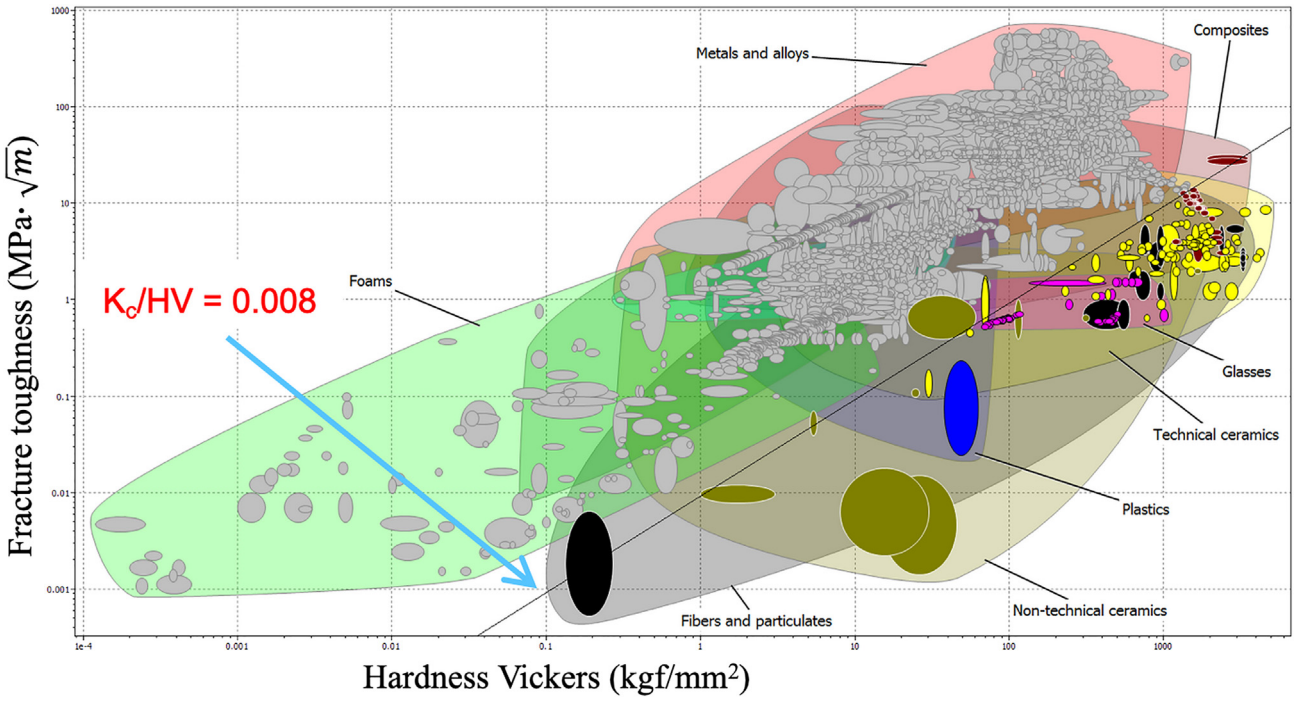

Fig. 7. Ashby selection chart identifying those materials with $K_c/HV < 0.008$, which is the estimated minimum threshold for having unstable crack propagation during a pillar splitting experiment.

of 100 μm. It is clear from this plot that, even using a cube-corner indenter, the pillar splitting method is limited to technical and non-technical ceramics, brittle glasses and (in a few cases) ceramic-matrix composites.

The limitation related to FIB milling could be overcome by using other machining methods to produce larger pillars, which would also expand the method's applicability to high temperature testing in which materials exhibit greater plasticity and toughness.

3.5. Applications

So far, we presented the key elements for the extraction of the fracture toughness using the pillar splitting method. In this section, we review some potential applications of the technique and explore the implications for practical design.

The first example we draw on is the work of Mughal et al. [38,39] in which pillar splitting was carried out on $Li_xMn_2O_4$ battery cathode materials in order to analyze the effect of state-of-charge (SoC) on fracture toughness. Remarkably, the authors managed to fabricate micro-pillars of crystalline oxides embedded in a polymeric matrix, see Fig. 8. Moreover, they found that K_c decreased as the SoC increased with an overall decrease of 53% from 0% SoC to 100% SoC (namely, from 0.26 to 0.49 MPa $m^{1/2}$) following a linear trend (Fig. 8c). The reason for the decrease has been associated with the reduction of Li^+ and Mn^{4+} ions, and also with the reported change of the lattice parameter. This study has clear implications for practical design of batteries by providing useful data for micromechanical models to predict cathode life cycle and the overall battery performance.

A similar approach was used by Wang et al. [37], who studied the fracture toughness of garnet structured Al-substituted $Li_7La_3Zr_2O_{12}$ (Al:LLZO) which is a solid state electrolyte with high ionic conductivity that is a promising candidate for all-solid-state lithium batteries. They found that the local K_c value obtained via micro-pillar splitting tests was 0.99 ± 0.05 MPa $m^{1/2}$, which is in good agreement with the reported global toughness value of 1.19 MPa $m^{1/2}$. Liu et al. [40] studied the mechanical properties of aluminosilicate (N440) fibers used to reinforce SiC matrix. Specifically, they managed to mill micro-pillars in the fiber and matrix separately to carry out local tests. Using this approach, the fracture toughness of the SiC matrix and the N440 fiber were found to be 2.26 ± 0.07 and 2.85 ± 0.04 MPa $m^{1/2}$, respectively. These results further validate the quality of the method, whilst expanding its applicability range for different classes of materials with complex architecture, such as composites.

More recently, the method was demonstrated to be capable for high-throughput statistical characterisation of heterogeneous materials and coatings in real industrial environments. In the recent work by Bolelli et al. [41], micro-pillar splitting method was used to monitor the evolution of fracture toughness of a Thermally Grown Oxide (TGO) layer in a thermally sprayed YSZ/NiCoCrAlY Thermal Barrier Coating (TBC) multilayer system subjected to thermal cycling fatigue. A critical thickness for the TGO was identified for the first time, above which the fracture toughness of the TGO decreases remarkably.

In another recent paper [42], the high-temperature fracture toughness of industrial PVD hard coatings was evaluated by micro-pillar splitting over a wide range of temperatures from RT to 500 °C. It was shown that, compared to ion-beam notched geometries, this approach reduces the likelihood of Ga^+ ion implantation during specimen preparation and is therefore a highly suitable method for ceramics fracture testing at high temperatures.

4. Micro-cantilever testing

4.1. Introduction

As early as 2005, indentation experiments using micro-cantilever geometry were reported for coatings by Di Maio and Roberts [43], and for TiAl alloys by Halford et al. [44]. The original approach was then applied to various geometries, testing conditions, sizes and materials. Different geometries such as cantilevers, double-cantilevers and clamped beams were tested in many studies. The results of fracture toughness evaluation obtained using different geometries were compared to each other, e.g. for Si by Jaya et al. [45]. In the following discussion of micro-cantilever testing we report different specimen geometries reported in literature, and review their application to determining the

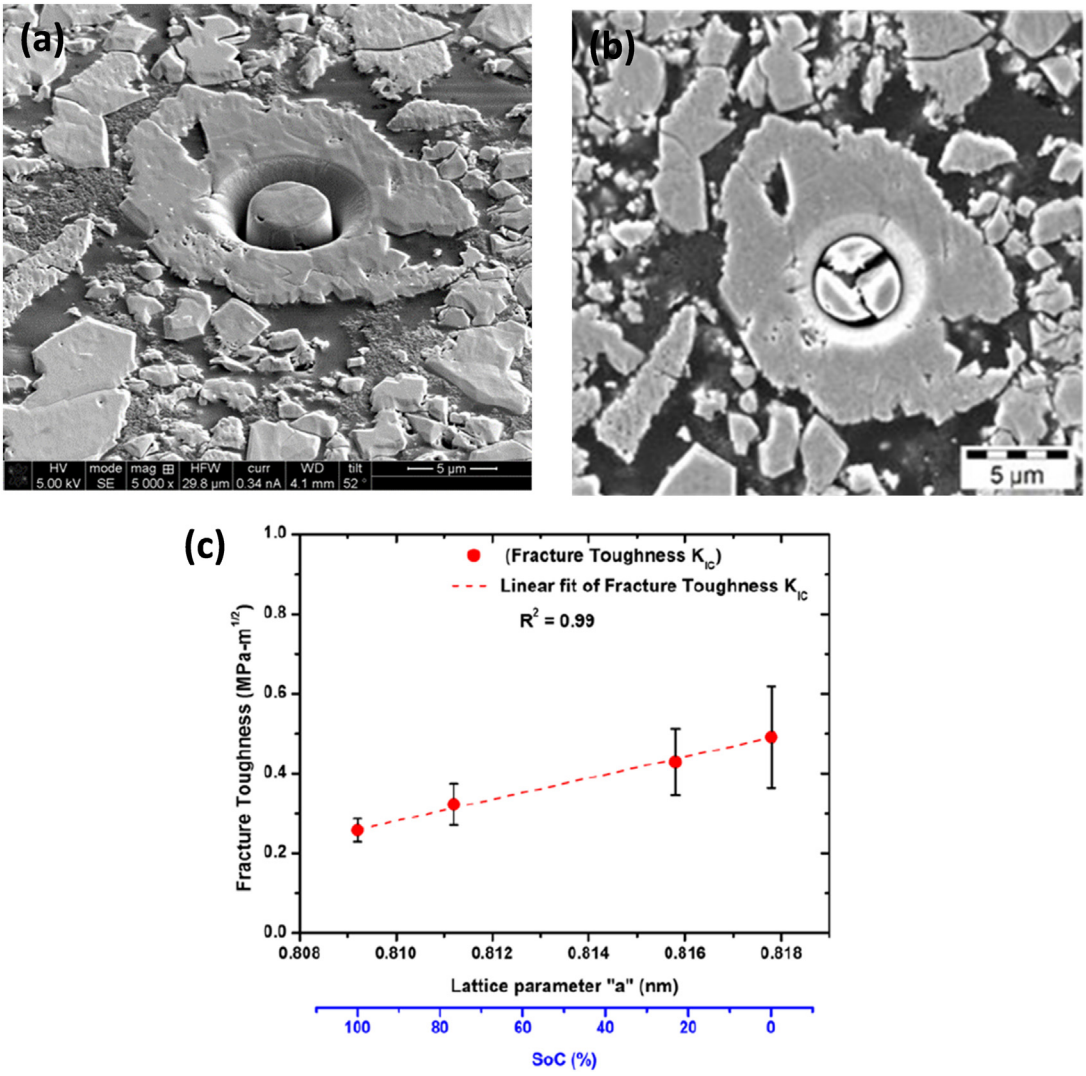

Fig. 8. (a, b) FIB-milled micro-pillars before and after splitting of $Li_xMn_2O_4$ crystals embedded in polymeric matrix; (c) fracture toughness as a function of lattice parameter [39]. Reproduced with permission from reference [39].

properties of individual phases and testing in harsh environments. Based on our own work, we present the application of LEFM CTOD and EPFM approaches to the evaluation of fracture toughness of NiAl.

4.2. Specimen and notch fabrication

With the flexibility of FIB-SEM instruments enabling a variety of possible testing setups, many different cantilever geometries have been reported in literature. Often FIB milling was used solely for sample preparation, although the use of other techniques has also been reported, e.g. chemical etching [46], femtosecond laser ablation [47] or micro electrical discharge machining [48], allowing efficient manufacture of specimens. Fig. 9 provides an overview of a few studies with different cantilever geometries and notching techniques. Rectangular beams are the most commonly used geometry. However, due to the need for FIB undercuts, those cantilever types can typically only be prepared at free sample surfaces. As presented by Di Maio and Roberts [43], Armstrong et al. [49] and Žagar et al. [50], beams can also be placed in the center of a sample piece, producing pentagonal or triangular cross-sections. Notches are also frequently milled by using FIB, as shown in the examples in Fig. 9. However, natural cracks can also be used in rare cases, as demonstrated by Wurster et al. [51], who prepared cantilevers with FIB notches, compared the measured fracture toughness to specimens with natural cracks, and concluded that good (sharp) FIB notches lead to similar fracture toughness values. There have been manifold successful attempts reported in relation to the notch design. Usually straight through FIB notches are used, as shown in Fig. 9b. However, thin ligaments or material bridges close to the free cantilever surfaces have been proposed [46] to produce sharp starter notches in brittle materials. Detailed investigations on how to perform tests in this case are reported in [52]. Also chevron-notches are used in rectangular [53] and triangular beams [50,54], and even in a bowtie micro-beam, as shown by Cui and Vinci [55] to create stable crack propagation in brittle materials such as fused silica, alumina, and Si. The effects of notch milling currents and ion types on fracture toughness were investigated by Best et al. [56]. They found that fracture toughness varied when Xe- or He-ions were used instead of Ga-ions, and discussed this finding in terms of the interaction of ions with the sample material. However, it should be noted that there is agreement that the notch depth and tip radius are factors of principal importance when it comes to fracture toughness determination.

4.3. Finite-element simulations of crack and cantilever design

Finite element (FE) modelling serves as an important technique for the development of testing geometries, the corresponding geometry functions, and the understanding of the effects of aspect ratios and notch geometries, as well as material plasticity. Cantilever dimensions

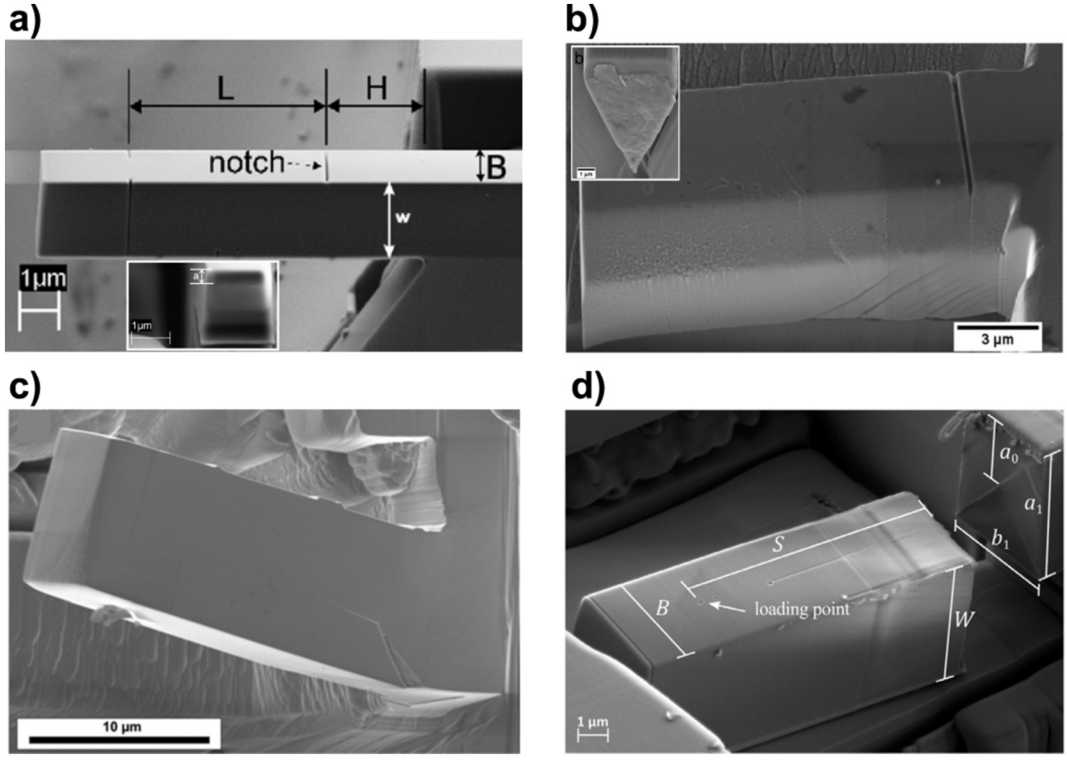

Fig. 9. SEM images taken from literature to show different cantilever and notch configurations for fracture toughness testing. (a) Oxide beams fabricated by a combined approach using wet-chemical etching and FIB; a crack with constant crack length is introduced by FIB with thin remaining material bridges at the free surfaces to produce sharp starter cracks, after [46]. (b) Pentagonal cantilevers with straight through thickness notches in Cu to test Bi-embrittled grain boundaries, after [49]. Rectangular cantilevers with (c) a natural pre-crack (not prepared by FIB) in a tungsten single crystal after testing, after [51] and (d) a chevron-notch prepared in fused quartz after testing, after [53]. Reproduced with permission from references [46], [49], [51] and [53], respectively.

tend to vary somewhat due to the use of FIB fabrication, therefore, validity must be ensured for the geometry functions that are used for fracture toughness evaluation. For rectangular cantilevers with a straight through notch it was shown that slight deviations in width, thickness and bending length do not significantly influence the geometry function of the micro-cantilever expressed in terms of the argument of crack length to width ratio [46,57,58]. In order to determine the dimensional effects, e.g. the influence of the thickness to width ratio *B/W* on the geometry function *f(a/W)*, 2D FE simulations were performed for two different cantilever aspect ratios for NiAl, which were *H:L:W:B* = 2:5:2.1:1.7 and 2:5:2.1:1.3 as shown in Fig. 10. Matoy et al. [46] suggested to use the geometry factor for precise aspect ratios of *H:L:W:B* = 2:5:2.1:1.7. Due to FIB preparation it is almost impossible to control the dimensions perfectly. Therefore, different aspect ratios as well as moment arms were simulated to see if these could affect the resultant geometry factor values. The calculated geometry factors *f(a/W)* were quite consistent, and the derived cubic polynomial expression for the geometry function is:

$$f(a/W) = 1.52 + 24.18\cdot(a/W) - 48.42\cdot(a/W)^2 + 77.61\cdot(a/W)^3 \qquad (14)$$

The geometry function shows very good agreement with literature values given in [46,58] and demonstrate that small deviations of the aforementioned aspect ratios do not exert significant influence. This allows the cantilever geometry to be used for a broad spectrum of dimensions. This was also confirmed by Brinckmann et al. [59], who investigated the influence of elastic anisotropy on the calculated geometry function values. Their conclusions were that for metals with moderate anisotropy, the difference from isotropic material behaviour amounted to <5%. Furthermore, the error due to anisotropy was of the same order of magnitude as deviations originating from geometrical inconsistencies due to FIB milling.

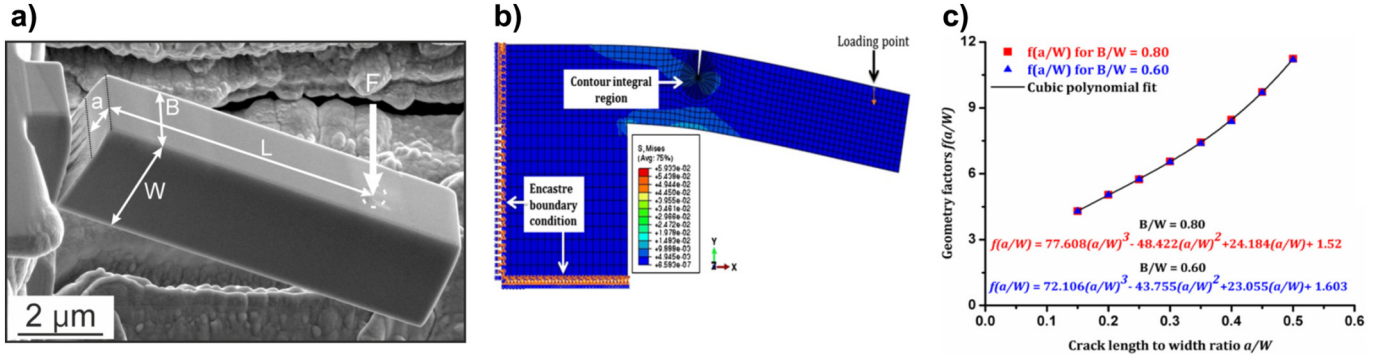

Fig. 10. (a) SEM image of a fractured cantilever in a NiAl single crystal, (b) FE model for the determination of the geometry function, shown in (c) for different a/W aspect ratios [57]. Reproduced with permission from reference [57].

However, as shown by Mueller et al. [53] and Žagar et al. [50], for chevron-notched specimens the effects of geometry can be more severe, and compliance calibration curves need to be acquired for each specimen to account for precise dimensions.

As illustrated in Fig. 11a, Brinckmann et al. [52] performed a large number of FE simulations to investigate the effect of pre-crack geometry on the apparent fracture toughness in the case of brittle material behaviour. The results are important for two reasons. Firstly, the preparation

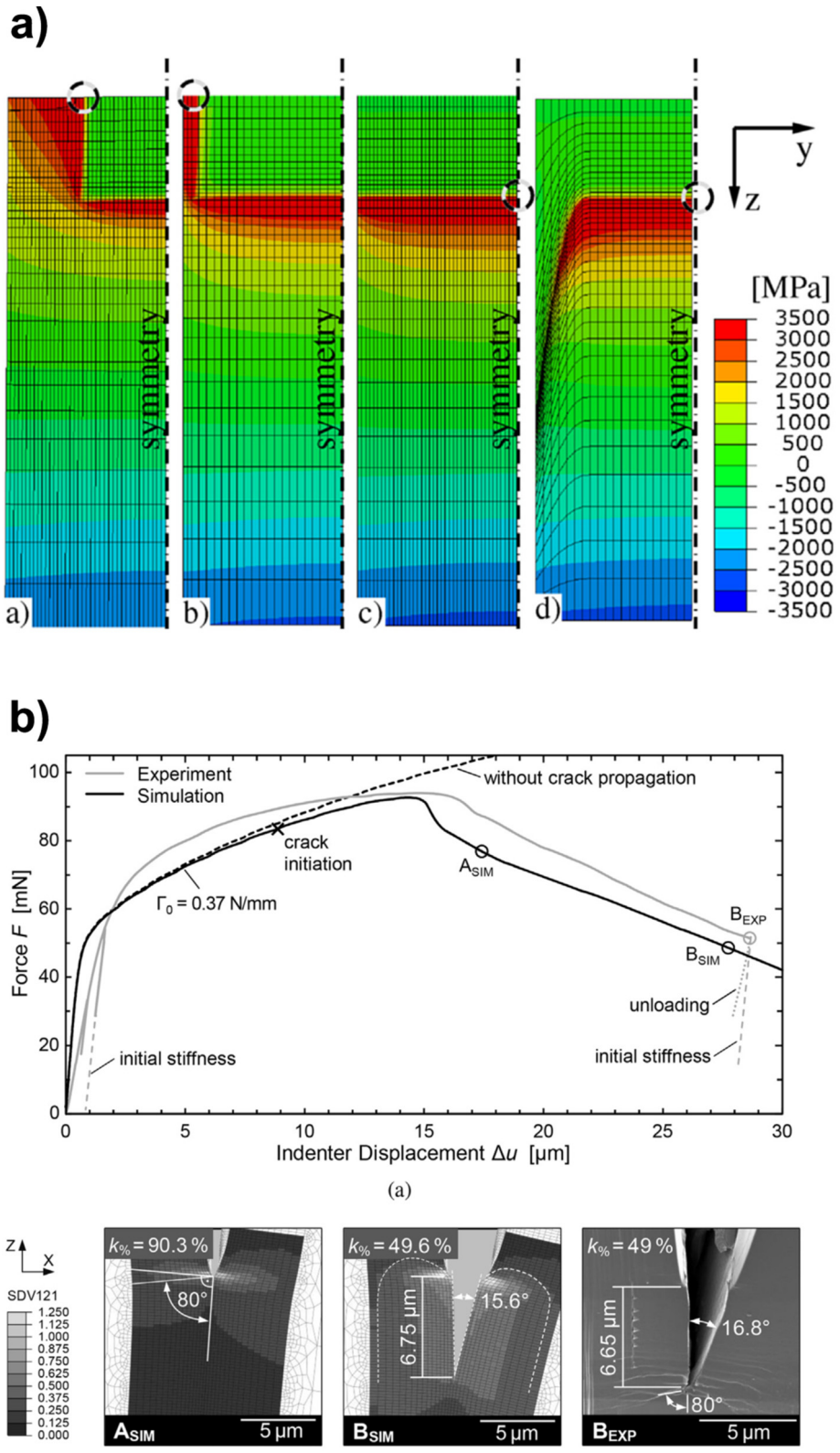

Fig. 11. FE simulations as tool to guide crack design and link simulations with experiments. (a) Effect of material bridges, straight through notch and "over-fibbing" on the (σ_{11}) stress distribution ahead of a crack in a rectangular cantilever, after [52] and (b) comparison of simulated and experimental fracture data of chevron-notched tungsten single crystal cantilevers showing plastic deformation and stable crack propagation, after [48]. Reproduced with permission from references [52] and [48], respectively.

of straight-through notches may intentionally or unintentionally result in rounded pre-crack corners or remaining material bridges. This may also imply non-uniform crack length and crack length to specimen width ratio, typically not accounted for in geometry function determination using 2D models. Secondly, the stress distribution at the crack tip depends on the exact shape of the pre-crack and defines the point of crack initiation and instability. Therefore, precise knowledge of maximum stress location is important.

FE simulations can also be used for comparison with experimental data. An example concerns crack growth and crack tip plasticity in confined volumes, as studied for tungsten single crystals by Bohnert et al. [48], illustrated in Fig. 11b. The finite element model was based on crystal plasticity constitutive law to mimic small-scale deformation behaviour, also containing cohesive zone elements, which are placed in the crack ligament. This enabled crack growth prediction for different notch types as a function of cantilever geometry.

4.3.1. Cantilever stiffness and stable crack growth

During cantilever bending, cleavage and instantaneous cracking may occur for many brittle materials. Once plastic yielding or other energy dissipating processes happen at the crack tip, stable crack growth is generally observed. These phenomena can be analysed by measuring the stiffness of the cantilever during the experiment: a growing crack corresponds to an increase in the *a/W* ratio, and decreasing bending stiffness.

The correlation between notched cantilever stiffness and the *a/W* ratio, based on FE calculations performed in [60], is shown in Fig. 12a, for a rectangular cantilever with the particular geometry given by *H:L:W:B* = 2:5:2.1:1.7. For comparison, the analytical solution of a clamped rectangular beam with corresponding dimensions is also shown, with the correlation between the stiffness k and the geometrical dimensions calculated according to beam theory:

$$W' = W - a = \sqrt[3]{\frac{4kL^3}{BE}}, \tag{15}$$

The stiffness values for the two geometries were normalized with respect to the maximum value. It is apparent that decrease in stiffness with increasing *a/W* ratio that is visible for both approaches is more pronounced for the clamped beam, which is explained by the existing support for the notched cantilever. Here, the width *W* is reduced by the respective notch length. Only at very large *a/W* ratios when both structures become very slim, the stiffness values are comparable. It is concluded that the stiffness reduction due to the change in the *a/W* ratio representing crack growth depends strongly on the boundary conditions and sample geometry.

It is also apparent that the use of clamped beam analytical solution underestimates the crack growth significantly. For various stiffness decreases, the notched configuration always provides larger *a/W* ratios and hence returns larger crack lengths than the analytical solution. This re-emphasizes the need for detailed knowledge of the geometry and model boundary conditions to determine correct crack length from stiffness values. A 2D model is only valid for a homogeneously advancing crack front: if the crack front is not straight, then more sophisticated models must be used to obtain correct effective stiffness values, in agreement with the conclusion by Alfreider et al. [61] who performed similar investigations. Additionally, they tested the predictions of their model for various materials and microstructures, and found good agreement between their adapted model and experimental stiffness measurements.

4.4. Testing of individual microstructural components

One of the big advantages of micro-scale over macro-scale mechanical testing is the possibility of testing single microstructural constituents. Materials with complex or hierarchical microstructures such as

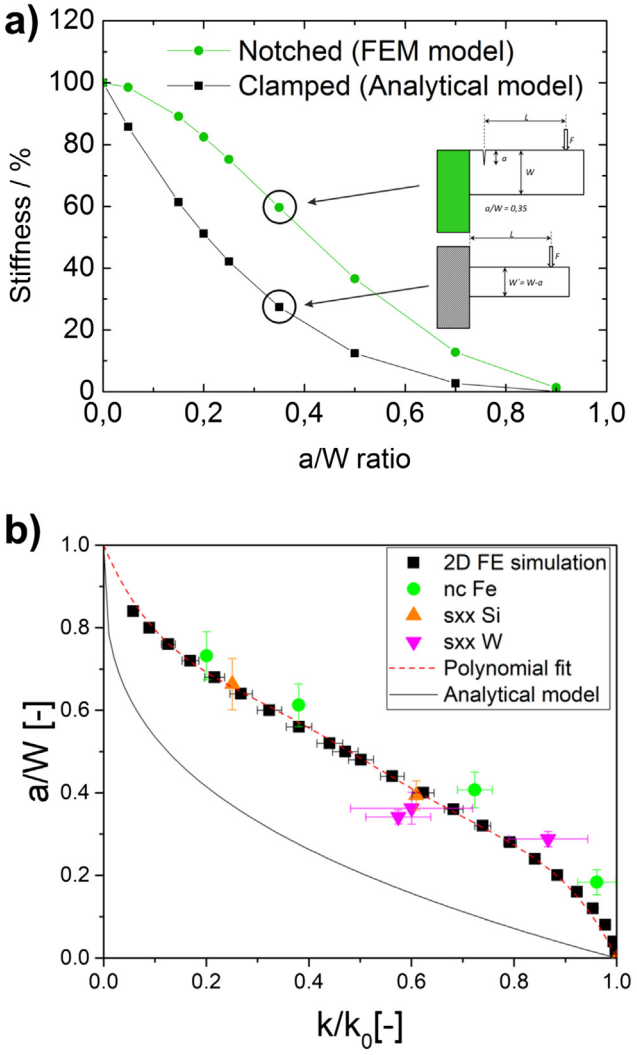

Fig. 12. FE simulations to correlate cantilever stiffness with crack length for specimens with straight-through notches: (a) Stiffness decrease as a function of individual *a/W* ratios for the tested geometry, where the support is ca. four times thicker than the thickness *B* of the cantilever and for the analytical solution of a fixed beam according to Eq. (15), after [60]. In (b) it is shown how simulation results match experimental data for different materials and *a/W* ratios [61]. Note that the axes are switched in (b) with respect to (a). Reproduced with permission from references [60] and [61], respectively.

polycrystals, composites, or bones can be investigated in detail using local testing techniques. On the other hand, the simplest case of a single crystal with known crystallographic orientation can also be considered. Tungsten is a model material with nearly perfect elastic isotropy and a semi-brittle behaviour. As a consequence, many fracture studies using micro-cantilevers focused on investigating the response of tungsten. Wurster et al. [51] were the first to develop a J-Integral procedure adapted to the micro-scale, in order to analyze semi-brittle fracture processes and calculate the fracture toughness of materials with non-negligible plastic zones. Combined numerical and experimental investigations on W single crystals were performed by Bohnert et al. [48,62] and Schmitt et al. [63] by means of micro-cantilevers. The aim was to determine the fracture toughness and to describe the local fracture behaviour of their specifically oriented specimens. Armstrong and co-workers studied the mechanical properties of ion-irradiated W [64], also investigating the fracture properties and finding a clear correlation between ion implantation and fracture toughness, which lied in the range of 5–10 MPa $m^{1/2}$. Ast et al. [65] and Alfreider et al. [61] studied crack initiation in W single crystals and determined continuous crack resistance curves. Due to non-negligible crack tip plasticity depending

on specimen orientation and sample size, efforts were also made to understand the evolution of plastic zones by means of in situ high-resolution electron backscatter diffraction (HR-EBSD) measurements [66,67]. Size-dependent fracture toughness and crack resistance behaviour were studied [65].

To investigate fracture of individual grain boundaries, Kupka and Lilleodden [68,69] performed notched micro-cantilever bending experiments in combination with finite element (FE) simulations. They determined critical fracture loads and characteristic stiffness values, which were normalized by means of simulations carefully adapted to the experiments. Armstrong et al. [70,71] used micro-cantilevers to understand stress corrosion cracking and oxidized grain boundaries. Graded (Pt, Ni) Al bond coats were investigated with respect to local fracture toughness determination by Jaya et al. [27]. The authors used a combined experimental and modelling approach to calculate the fracture toughness in individual zones of the coating by means of edge-notched doubly clamped micro-beams and discussed amongst others the effects of sample geometry and the local microstructural changes on their results. Webler et al. [72] investigated the effects of local chemical gradients on the fracture toughness in NiAl bond coat systems. They performed electron-backscatter diffraction mapping of the coatings and milled specimens in differently oriented grains. Due to thermal treatment, gradients in chemical composition were achieved, and fracture toughness was determined as a function of local chemistry and cantilever orientation.

Not only coatings and thin films are of interest in current research. It is worth drawing on a further example of microstructural component testing, namely, single interfaces investigated by Matoy et al. [73]. They determined critical energy release rates for different interfaces between silicon oxide and a metallic thin film. Micro-component interfaces were also intensively studied by Hirakata et al. [74], Kawei [75] and Takahashi et al. [76]. They considered interface plasticity and crack initiation between a brittle Si substrate and a thin plastically deforming Cu layer in situ in the transmission electron microscope (TEM), and determined the stress distribution at the interface in combination with FE modelling.

Hydrogenated amorphous carbon (a-C:H) coatings and interfaces were studied by Schaufler et al. [77]. The interfacial fracture strength and toughness of two a-C:H coatings with Cr adhesion layer on a steel substrate were determined directly using micro-cantilever bending experiments as shown in Fig. 13. The coating conditions for the two systems were essentially the same, only slight modifications were made in the adhesion layer. These changes resulted in an entirely different delamination behaviour, ranging from HF1 (excellent) to HF6 (poor adhesion) according to the Rockwell C adhesion test. The well-adhered interface between the adhesion layer and the a-C:H was found to have a fracture strength and toughness value close to the a-C:H coating itself. Changing the process conditions reduced the bending strength by ~40%, leading to strong delamination and a catastrophic behaviour during Rockwell C testing. An interfacial fracture toughness value of ca. 2 MPa $m^{1/2}$ was found for the well-adhered coating, exceeding even that of pure a-C:H.

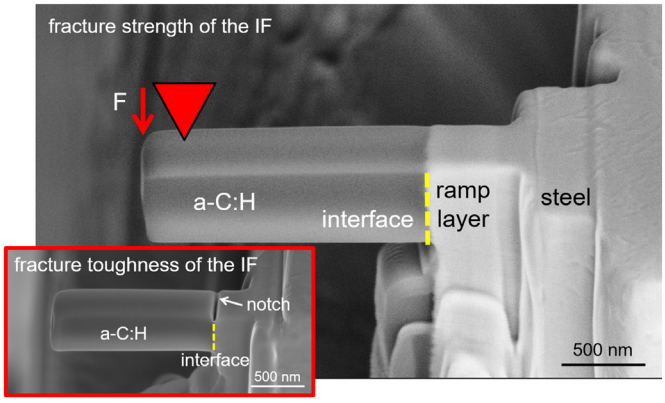

Fig. 13. SEM images of micro-cantilevers prepared for fracture strength and toughness testing of the interface between a-C:H and the Cr bond coating [77]. Reproduced with permission from reference [77].

4.5. Adaptation of testing conditions to realistic environments

For many applications it is insufficient to perform mechanical tests quasi-statically, in air or vacuum at room temperature. Strain and loading rate effects, temperature and the testing environment may significantly alter the fracture behaviour in terms of fracture initiation and propagation. Hydrogen-assisted cracking and hydrogen embrittlement were investigated by Costin et al. [78], Deng and Barnoush [79] and Rogne et al. [80]. In Fig. 14a it is shown how hydrogen embrittles the specimens, reducing crack tip plasticity, as demonstrated by EBSD analysis. When specimens were tested in vacuum in the absence of hydrogen, significant crack tip opening displacements were observed in the SEM images accompanied by significant plastic deformation associated with an increase in the kernel average misorientation (KAM) angles observed. Local micron-scale testing approaches are needed to correlate hydrogen-affected crack kinetics with specific microstructural constituents. Only by testing selected, well-defined and representative material volumes of small size can effects such as hydrogen embrittlement be

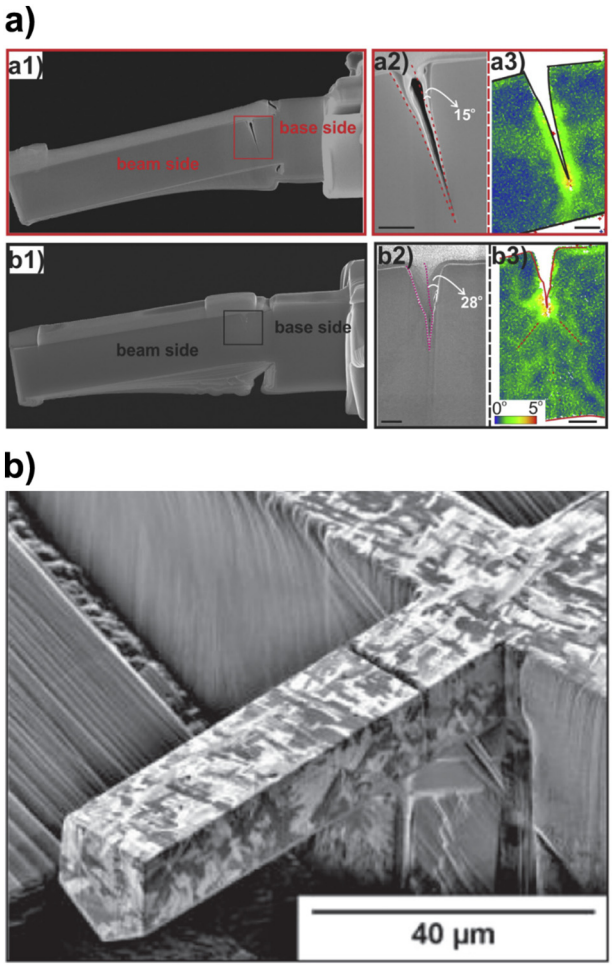

Fig. 14. Hydrogen embrittlement and hydrogen-assisted cracking are important research fields and local fracture approaches are needed to understand the interaction of cracks with microstructure. (a) SE micrographs and EBSD measurements on FIB prepared cross-sections of single crystals of the intermetallic compound FeAl showing a more brittle failure in the case of hydrogen charging, a1)–a3), and a more ductile behaviour, when specimens are H-free, b1)–b3), after [79]. The shown scale-bar is 500 nm. (b) Ion-induced SE micrograph of a micro-cantilever in acicular ferrite before testing to investigate its intrinsic susceptibility to hydrogen-assisted cracking, after [78]. Reproduced with permission from references [79] and [78], respectively.

understood. Takahashi et al. [81,82] studied hydrogen embrittlement inside an environmental TEM and noticed that the fracture process became more brittle when the amount of hydrogen gas was increased. They investigated grain boundaries in polycrystalline Ni_3Al samples and Si—Cu interfaces.

Temperature effects on fracture behaviour were discussed by Best et al. [34] for CrN coatings. They conducted both micro-cantilever and micro-pillar splitting, as well as double beam cantilever tests up to 500 °C, and discussed the effects of Ga-ion notching and Ga diffusion at elevated temperatures on fracture toughness. Jaya et al. [83] investigated the brittle-to-ductile transition (BDT) behaviour of Si single crystals at the micro-scale, and found a gradual increase of fracture toughness with temperature. Fracture initiation and temperature effects on the fracture of Si beams were also studied by Hintsala et al. [28], who found a steady increase in the critical stress intensity factors from 300 °C upwards. Crack resistance behaviour and fracture toughness were analysed for α-Fe single crystals by Snartland et al. [84] for different crack systems at room temperature and −75 °C. Ast et al. [58] investigated the BDT behaviour of tungsten single crystals in the temperature range from −90 °C to 250 °C at the micro-scale. It could be shown that increased temperature enables thermally activated processes and plays a decisive role in fracture mechanics in the context of crack tip plasticity in confined volumes.

For further reading on recent progress in small-scale fracture testing, the reader is referred to two recently published review articles by. Dehm et al. [85] and Pippan et al. [86] discuss in detail the fundamental aspects, that need to be considered when conducting small-scale fracture tests.

In the following section, the importance of the plastic zone and its interplay with specimen dimensions and the microstructure are addressed in more detail.

4.6. The influence of the plastic zone on fracture in micron-sized specimens

According to Irwin [5] the plane strain plastic zone radius r_{pl} in front of a crack tip in a homogeneous material is given by:

$$r_{pl} = \frac{1}{3\pi}\left(\frac{K_I}{\sigma_y}\right)^2 \tag{16}$$

The macroscopic yield stress σ_y and the stress intensity factor K_I determine the formation of the plastic zone decisively. In macro-scale specimens like compact tension (CT) samples, Fig. 15a, the process or plastic zone is small with respect to the sample geometrical dimensions. Only at the free surfaces a stress state develops that approaches the plane stress idealisation.

Upon miniaturizing the specimen to micron dimensions, the size of the plastic zone may become comparable with that of the specimen. For brittle materials, Fig. 15b, generally characterised by low fracture toughness and high yield or fracture strength, this plastic zone is negligible, and inter- or trans-granular cleavage fracture dominates. Certain semiconductors, bcc metals and also biomaterials show fracture patterns influenced by thermally activated deformation at the crack tip, Fig. 15c. Extrinsic parameters like temperature and loading rate, as well as intrinsic parameters like crystallographic orientation, purity, fiber orientation etc. determine the fracture and deformation behaviour by influencing yield strength and fracture toughness. For most metals, Fig. 15d, the plastic zone becomes so large that fracture is inhibited due to enhanced crack tip plasticity. Therefore, small-scale yielding (SSY) approximation in fracture mechanics cannot be applied anymore.

In the following, the scenario presented in Fig. 15c will be treated in more detail in the particular context of micro-cantilever geometry. Fig. 16a illustrates that depending on sample size, the plastic zone may cover only a small portion of the sample volume in larger samples (see cantilever 1).

With decreasing sample size and under the assumption of a size-independent yield stress, the theoretical plastic zone according to Eq. (16) expands through a significant portion of the specimen (cantilever 2). Finally, upon further miniaturization the plastic zone spreads over the entire specimen. Dislocations are able to leave the crystal at all free surfaces, changing thus the mechanical response of the sample and the stress state. It is known from micro-pillar compression testing that the yield and flow stresses tend to increase when the sample dimensions are decreased [87–92]. The size of the plastic zone which depends on the yield stress according to Eq. (16), is consequently decreased when the dimensions reach a critical length. For small-scale samples, microstructural effects in combination with inhomogeneous loading conditions and strain gradients must also be considered. Plastic strain gradients acting at the crack tip and creating large shear strains

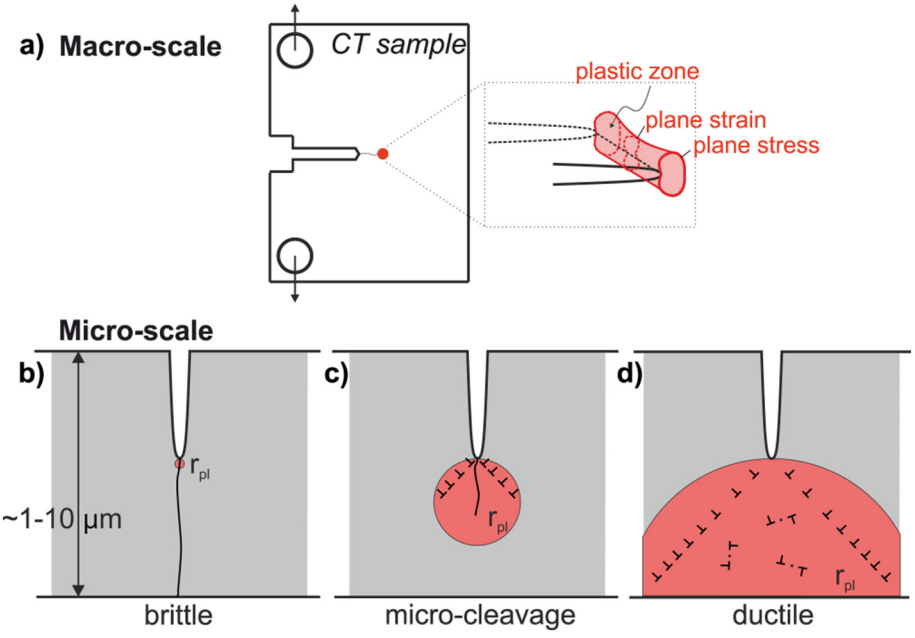

Fig. 15. Schematics for the description of the plastic zone ahead of the crack tip (a) in a compact tension specimen and in a single crystal (SX) micron-scale specimen showing (b) brittle fracture, (c) dislocation-controlled micro-cleavage and (d) an entirely ductile behaviour with dislocation nucleation from the crack tip and from active sources.

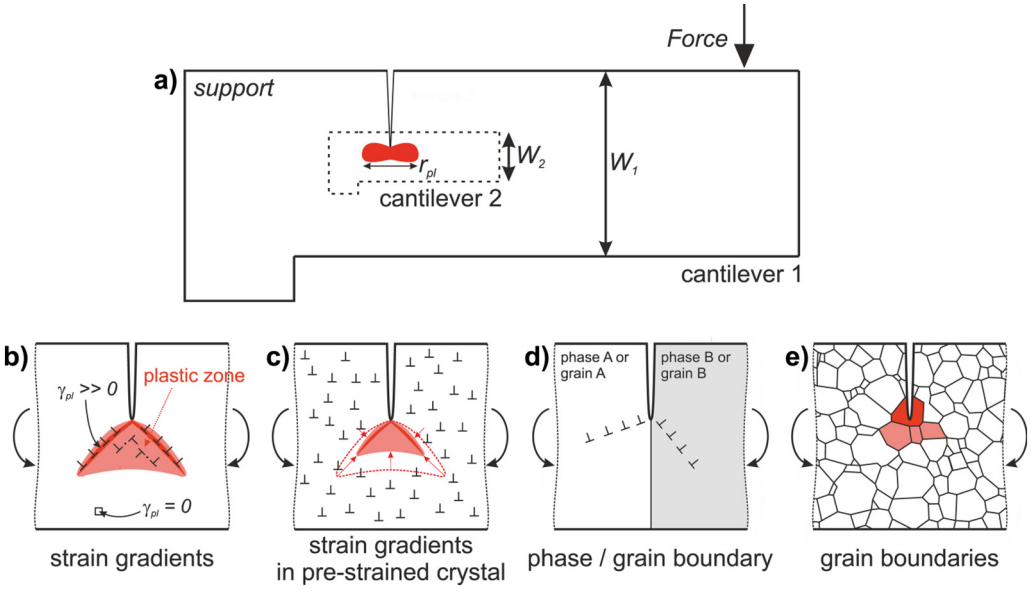

Fig. 16. The development of plastic zones in loaded micro-cantilevers: (a) although cantilever size may change, plastic zone size remains the same for given severity of loading, (b) strain gradient effects, (c) effect of additional plastic pre-straining, (d) testing of single phase or grain boundaries and (e) testing of multiple grains; after [65]. Reproduced with permission from reference [65].

γ_{pl} (Fig. 16b) can become important once the sample dimensions are significantly decreased [93]. Furthermore, an increased inherent dislocation density (Fig. 16c) can additionally affect plastic zone expansion. Grain boundaries (Fig. 16d and e) acting as obstacles for dislocation motion may also affect crack tip plasticity and are known to influence the fracture behaviour strongly [68].

4.7. Fracture mechanics analyses of notched micro-cantilevers

4.7.1. Evaluation according to LEFM

In order to determine reliably the plane strain fracture toughness K_{Ic}, according to linear-elastic fracture mechanics (LEFM), several requirements must be fulfilled specified in various standards [94–96]. Ideally, atomically sharp notches have to be investigated, obtained by fatigue pre-cracking, which is often not possible at micron length scales. Fracture toughness values are generally referred to as "qualified" values at this scale, and presented with the subscript "q" to indicate that not all conditions were fulfilled. According to [94], fracture toughness can be determined as follows:

$$K_{Iq,LEFM} = \frac{F_q L}{BW^{3/2}} f(a/W) \tag{17}$$

The geometrical dimensions are illustrated in Fig. 10a. The critical load F_q can be determined according to [95], L is the moment arm between the notch and the loading point or line (when a wedge-type indenter is used, e.g.), B is the beam thickness, W is the beam width and $f(a/W)$ is a dimensionless geometry function that can be determined for various notched beam geometries analytically or by FE simulations [46,57].

4.7.2. Evaluation according to EPFM

4.7.2.1. Evaluation of the J-Integral. If the conditions for small-scale yielding stated in ASTM standard E 399 [95] are not fulfilled, elastic-plastic fracture mechanics (EPFM) needs to be chosen to describe fracture behaviour. The reason is that the plastic zone is too large for reliable determination of fracture toughness according to LEFM. One technique, which was adapted to the micro-scale for the first time by Wurster et al. [51], is the J-integral technique. The approach conventionally applied for macroscopic testing and described in ASTM standard E 1820 is illustrated in Fig. 17a. Partial unloading segments are used after specific displacement intervals to determine the contact stiffness, from which the corresponding beam stiffness is then calculated. Decreasing stiffness is correlated with crack growth, with the quantity A_{pl} characterising the amount of dissipated plastic energy. Furthermore, for each cycle i, the current force F_q is recorded. Since certain geometrical requirements from the standard developed for macroscopic testing cannot be transferred to the micro-scale, the results are again denoted by the subscript "q".

By superimposing a constant amplitude sinusoidal oscillation of a few nm on the applied indenter tip displacement as illustrated in Fig. 17b, the contact stiffness can be measured continuously throughout the bending tests [68]. In this case one full oscillation represents a loading cycle. The J-Integral is calculated continuously, allowing a record of crack resistance curve (R-curve) to be obtained for materials showing plasticity during fracture [97].

The J-Integral consists of elastic and plastic parts, and can be determined for the i-th loading-unloading cycle using the following equation [94] for isotropic material:

$$\begin{aligned} J_{(i)} = J_{el,(i)} + J_{pl,(i)} = {} & \frac{(K_{Iq,(i)})^2 (1-\nu^2)}{E} \\ & + \left[J_{pl,(i-1)} + \frac{\eta (A_{pl,(i)} - A_{pl,(i-1)})}{B(W - a_{(i-1)})} \right] \\ & \times \left[1 - \gamma \frac{a_{(i)} - a_{(i-1)}}{(W - a_{(i-1)})} \right], \end{aligned} \tag{18}$$

where $K_{Iq,(i)}$ is determined as shown in Eq. (17), ν is Poisson's ratio, E is Young's modulus, η and γ are a constants, which depend on the geometry and which can be set to 1.9 and 0.9, respectively, for the single edge bend specimen. A_{pl} is defined as the area under the force-displacement curve excluding the elastic contribution.

Whether the J-Integral is determined continuously or by partial unloading sections, a continuous or discontinuous crack resistance curve can be generated, respectively. From such a curve, a critical J-Integral value J_q for the onset of stable crack propagation is determined. Various suggestions have been made about how to determine J_q at the micro-scale. Bohnert et al. [48] proposed to rely on the measurement

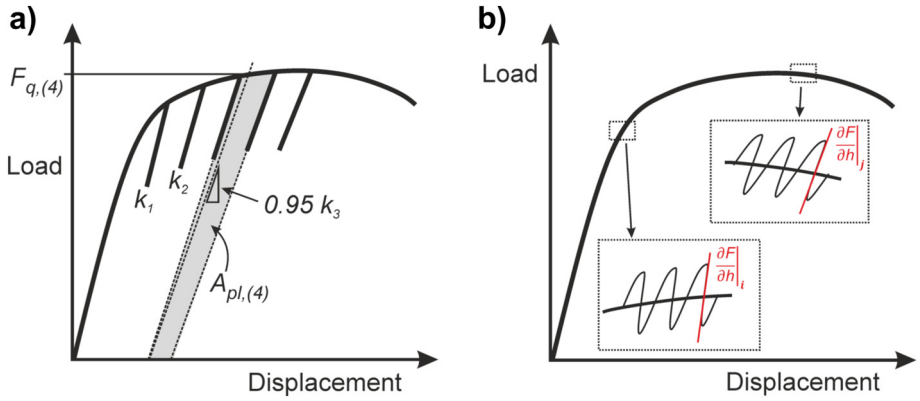

Fig. 17. Schematic load-displacement curves to describe the *J*-Integral testing procedure: (a) method with partial unloading segments to determine the contact stiffness k_i and the relevant quantities $A_{pl,\,(i)}$ and $F_{q,\,(i)}$ and (b) continuous stiffness technique which allows continuous recording of the contact stiffness. Reproduced with permission from reference [65].

of the crack tip opening displacement (CTOD), which they determine directly from SEM images of the deformed specimens. Using this technique, the construction or blunting line with the slope corresponding to the yield stress is shifted by half of the CTOD. The intercept of this line with the *R*-curve yields J_q. This promising approach based on a clear physical background was adopted in further studies [61,79]. However, it requires detailed knowledge of the blunting behaviour and the yield stress, with the further major drawback being that the blunting line is constructed in the FIB-affected region. Another approach is to determine the blunting line directly from the R-curve [51,60]. This requires the initial data trend to be linear, which may not always be the case. Pippan et al. [86] propose to adapt the fracture initation criterion to initial sample dimensions to make the definition of J_q scale-independent. Their idea is to construct the blunting line by means of 2% of the initial crack length. Finally, using a vertical line at a fixed point in the crack propagation (depending on the test length scale) offers an easy way of comparing specimens of similar size [97]. Once J_q is determined, the fracture toughness can be calculated according to:

$$K_{Iq,J} = \sqrt{\frac{J_q\, E}{(1-\nu^2)}} \tag{19}$$

4.7.2.2. Evaluation of CTOD. Another macroscopic EPFM testing technique that can be adapted to the micro-scale is the crack tip opening displacement (CTOD) method. According to the ASTM standard E1290 [96], the crack mouth opening displacement (CMOD) has to be determined in order to calculate a critical crack tip opening displacement $\mathrm{CTOD_c} = \delta_C$. For rather brittle materials this is characterised by the onset of unstable crack extension with no significant prior stable crack propagation. For a more ductile material having a pronounced plastic zone around the crack tip, this critical value can be estimated at the first attainment of a force plateau. Again, not critical but qualified values are derived, as certain standard requirements are not fulfilled. The CTOD is separated into an elastic and a plastic component similarly to the previous section for the *J*-Integral approach. The elastic part is again obtained by the LEFM formulations, whilst for the plastic part a hinge model is applied, as proposed in [98]:

$$\delta_q = \delta_{q,el} + \delta_{q,pl} = d_n \frac{(K_{I,0}.95)^2(1-\nu^2)}{\sigma_Y E} + \frac{r_{pl}(W-a_0)v_{pl}}{r_{pl}(W-a_0)+a_0}, \tag{20}$$

Here d_n is a dimensionless factor, which depends according to [99] on the strain hardening exponent n and on the ratio of σ_y/E, and σ_Y is an effective yield strength, which is half of the sum of yield strength and maximum flow stress. The hinge model incorporates the plastic rotational factor which is ca. 0.44 for the single-edge bend SE (B) geometry, and which can be applied for the cantilever geometry in the first approximation. From the recorded Force-CMOD curves the plastic part of the displacement v_{pl} is obtained by constructing a line parallel to the loading line. This procedure to determine δ_q values is called the basic test method and provides only an approximation for the fracture toughness in the case of a ductile material. More accuracy is achieved by R-curve testing, for which the stiffness needs again to be recorded. Fracture toughness can be calculated from the following equation, according to [96]:

$$K_{Iq,\delta} = \sqrt{\frac{\sigma_Y E \delta_q}{d_n(1-\nu^2)}}. \tag{21}$$

The determination of critical CTOD values strongly depends on the yield stress σ_y of the material, which can be strongly influenced by size effects at the micro-scale. It was shown for unnotched micro-cantilevers at the same length scale that smaller beams showed a higher yield strength than larger beams [100–102]. It becomes apparent that plastic deformation takes place in a very confined area. This leads to the generation of strong strain gradients in the case of bending of thin beams and to higher yield stresses in the samples.

4.8. Example of fracture toughness evaluation: soft and hard oriented B2-NiAl

In the following, we focus on the evaluation procedures for micro-cantilever bending experiments based on our previous work on single crystals of semi-brittle intermetallic compound B2-NiAl [57,60,97]. It is a suitable model material for understanding fundamental fracture processes in which plasticity is involved, and for establishing new evaluation techniques. Depending on orientation, NiAl may show brittle fracture at ambient conditions. Literature data from macroscopic fracture tests is available [103–105], which allows for comparison between different length scales. NiAl is anisotropic, and fracture toughness values are presented for "hard" and "soft" orientations for micro-cantilevers in Fig. 18.

For specimens loaded in the "soft" orientation along the ⟨110⟩ direction, values obtained are 3–4 MPa $\mathrm{m}^{1/2}$. K_{Ic} values of 5–7 $\mathrm{MPam}^{1/2}$ are reported for crystals loaded along the "hard" ⟨100⟩ orientation [104]. Lowest energy dislocations with a ⟨100⟩ Burgers vector cannot be activated, and a significantly higher yield strength is observed in experiments than when the sample is loaded along a soft orientation [106]. The cleavage fracture occurs on {110}-type planes, unlike for other body centered cubic materials like α-Fe, W and Cr etc. [103]. The ⟨110⟩ loading axis was chosen for testing the soft orientation.

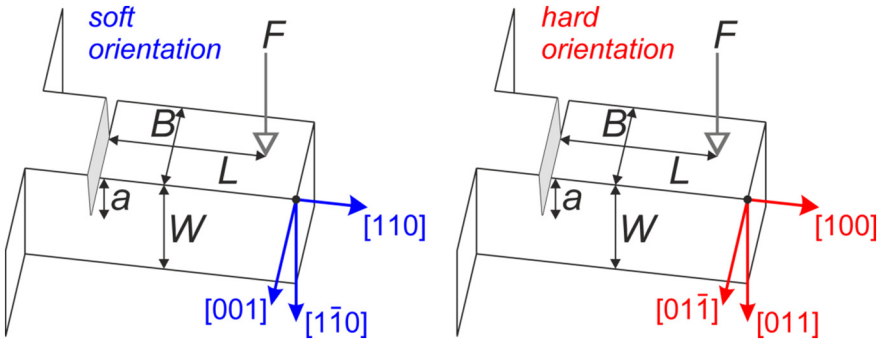

Fig. 18. Schematic drawings of microcantilevers with indication of the "soft" and "hard" orientation in NiAl single crystals.

4.8.1. Anisotropic stress field around loaded crack tips

As shown in Eqs. (18)–(21) only two elastic constants, E and ν, are needed in the case of isotropy. However, elastically isotropic material behaviour cannot always be assumed. The respective equations become more complex and contain elastic constants C_{ij} in the case of elastic anisotropy. In the following, an example is shown for cubic NiAl with the anisotropy factor of 3.7, and elastic constants given in Table 1.

In order to use EPFM for an anisotropic material, the factor $E/(1-\nu^2)$ in the case of plane strain, and E in the case of plane stress must be exchanged by factors denoted as $E^*_{plane\ strain}$ and $E^*_{plane\ stress}$, respectively. These factors take into consideration both the elastic constants and the orientation of the cantilevers. For the rectilinear anisotropic case, fracture toughness is calculated applying the linear-elastic stress theory for the field around a crack tip according to Sih and Liebowitz [108,109]:

$$K_{Ic} = {G_{Ic}}^{1/2}\left[\frac{S_{11}S_{22}}{2}\left\{\left(\frac{S_{22}}{S_{11}}\right)^{1/2}+\frac{2S_{12}+S_{66}}{2S_{11}}\right\}\right]^{-1/4}, \tag{22}$$

Here S_{ij} are the reduced elastic compliance constants in the case of plane strain and ⟨100⟩ crack orientation. When the crack and specimen orientation is changed, the coordinate system has to be rotated and the respective compliance constants have to be recalculated. The values for $E^*_{plane\ strain}$ and $E^*_{plane\ stress}$ for NiAl for the "soft" and "hard" orientation are also listed in Table 1.

4.8.2. Evaluation according to LEFM

Three load-displacement curves for micro-cantilevers in the soft orientation, tested in situ in the SEM and showing brittle fracture are presented in Fig. 19a. Due to slight variations in the sample dimensions, some of the cantilevers appear stiffer compared to others. By using Eq. (17), the load is normalized with respect to the sample geometry, deriving thereby the stress intensities for the different cantilevers. Good matches are observed for the initial elastic loading part, as shown in Fig. 19b. However, some scatter is apparent at larger displacements, where the deviation from the linear behaviour is seen. If only LEFM were applied, the final point of each curve would represent the respective K_{Iq} value. However, since $F_{max}/F_{0.95} > 1.1$ [95], LEFM is not applicable. However, fracture behaviour can be compared well between samples, and fracture toughness estimated to be $K_{Iq,\ LEFM} = 2.1 \pm 0.3$ MPa m$^{1/2}$.

Table 1
Overview of elastic constants of NiAl for the determination of E^* in plane strain and E^* in plane stress for the "soft" and the "hard" orientation [107].

C_{11} (GPa)	C_{12} (GPa)	$C_{44} = C_{66}$ (GPa)	$E^*_{plane\ strain}$ (GPa)		$E^*_{plane\ stress}$ (GPa)	
			Soft	Hard	Soft	Hard
199	137	116	170	195	125	151

4.8.3. Evaluation according to EPFM – J-Integral

The results of a slightly larger cantilever from a hard oriented NiAl crystal showing significant crack tip plasticity are shown in Fig. 20. Initially, there is a linear elastic loading segment followed by a remarkable hardening regime. The experiment was stopped at a bending displacement of ~6 μm. The continuously measured cantilever stiffness remained constant for the first 1.5 μm of displacement, which is beyond the elastic loadinging. Then it continuously drops during the course of the experiment indicating stable crack propagation. The fact that a

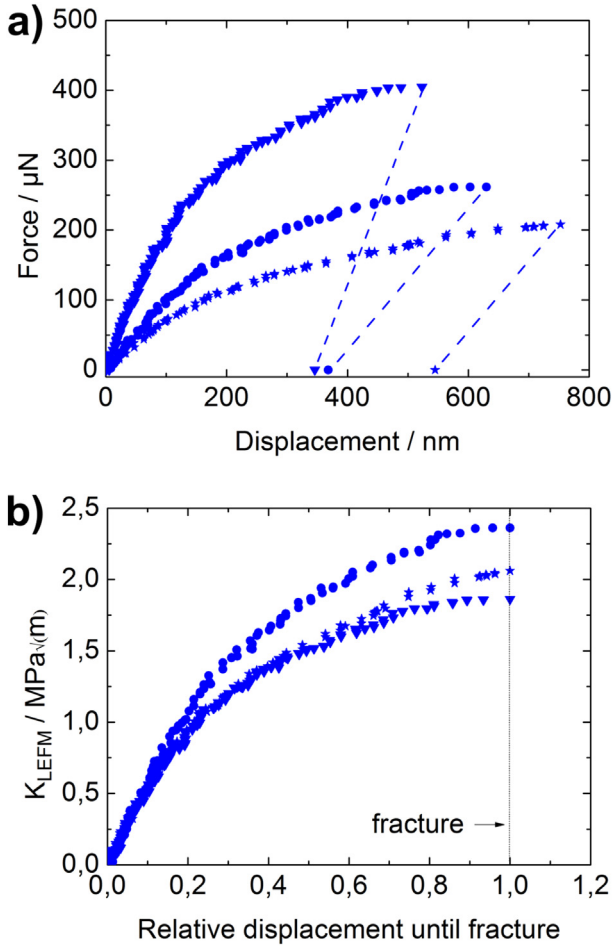

Fig. 19. (a) Force-displacement curves for soft-oriented cantilevers. The unloading slopes were estimated to be the same as the individual loading slopes. Slight changes in the geometrical dimensions like moment arm or beam width cause different force levels and displacements until the point of brittle fracture. Therefore, the respective stress intensity factors as a function of the "Relative displacement until fracture" are shown in (b). Reproduced with permission from reference [60].

drop in stiffness is linked to crack propagation can be confirmed by testing unnotched cantilevers. These cantilevers show a constant stiffness level in both the elastic and plastic loading sections of the experiment. Towards the end of the test, six partial unloading segments were performed. The corresponding cantilever stiffness data is illustrated as hollow square symbols in Fig. 20b. An excellent agreement is found between the two methods.

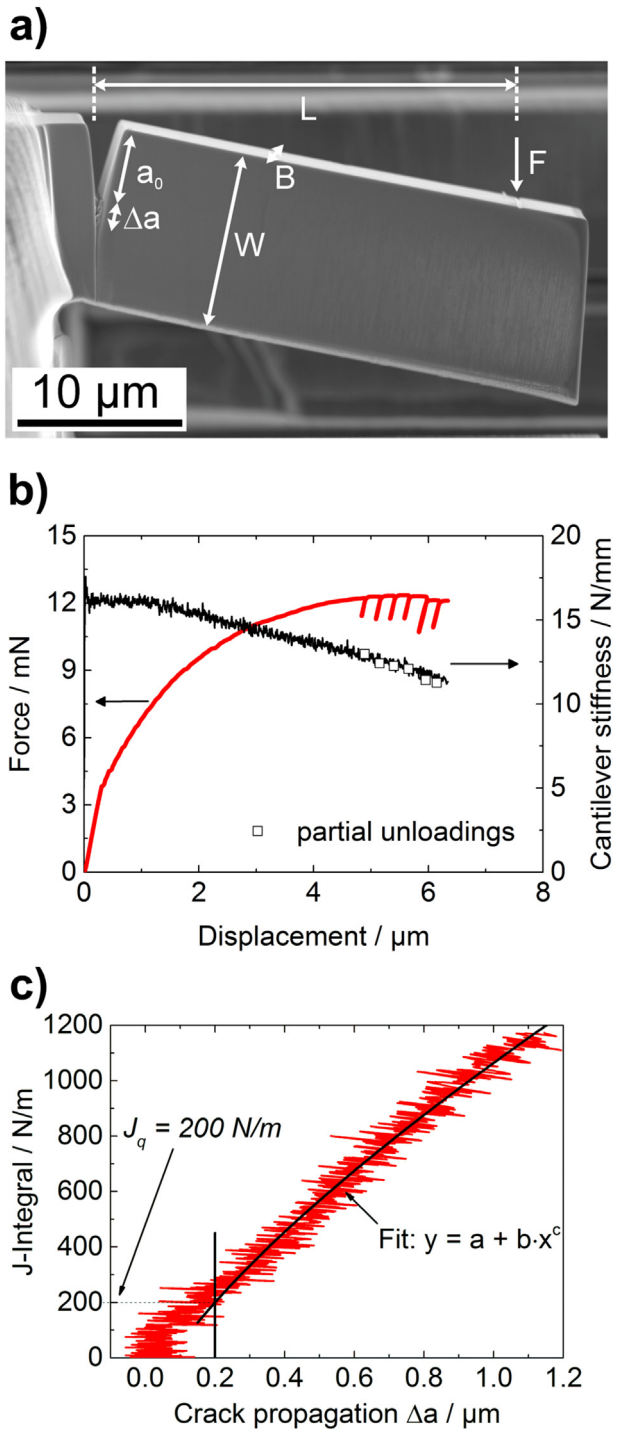

Fig. 20. (a) SEM image of a hard oriented NiAl cantilever after fracture, (b) load-displacement curve, continuous and discontinuous cantilever stiffness from continuous stiffness measurement (CSM) signal and partial unloading, respectively and (c) crack resistance curve with fit for the determination of J_q at a critical crack length of 200 nm. Reproduced with permission from reference [97].

Continuous crack resistance curves can be plotted as shown in Fig. 20c. A constant initial cantilever stiffness means that the crack length stays constant, and the *J*-Integral increases steeply in the beginning due to the plastic component. Once the stiffness decreases, the resistance to crack propagation rises and the crack propagates stably until the experiment is stopped. At that point the propagated crack length is calculated to be around 1.2 µm, which matches crack length measurements from SEM images after testing, as shown in Fig. 20a.

Presently there is a lack of standard procedures to define the onset of fracture from crack resistance curves. Pippan et al. [86] propose a practical approach to define J_q or J_i values with the help of blunting lines derived from macroscopic fracture testing. However, detailed knowledge of the crack tip blunting, the size-dependent yield stress and the slope of the *R*-curve in the blunting regime are required for this. As shown for NiAl in the hard orientation in Fig. 20c, it is difficult to define precisely the initiation of fracture. Therefore, a criterion of 200 nm of stable crack propagation was chosen and J_q was defined as the intercept of a vertical line and a fit according to the ASTM standard [94]. Although this definition is not meant to serve as a standard routine for the definition of fracture initiation, it allows for an easy and straightforward comparison of tested cantilevers of similar size.

4.8.4. Evaluation according to EPFM – CTOD

CTOD was measured indirectly by evaluating CMOD from in situ images or videos taken during testing in the SEM, as shown in Fig. 21. For the soft orientation, only limited CMOD and hence little crack growth was observed, followed by brittle abrupt failure. A more pronounced CMOD was observed for the hard orientation which displayed a constant force plateau. Since the geometries of tested cantilevers were quite similar, it is concluded that the crack mouth opens further for the hard orientation and higher forces are also achieved, in agreement with the results presented before. This leads to higher plastic CMOD v_{pl} and higher fracture toughness for the hard orientation, as shown in the overview plot in Fig. 22. A force plateau was reached for the hard orientation due to two opposing effects: strain hardening leads to a further increase in the force, but as crack growth takes place, cross-sectional area is diminished leading to a decrease in force. The basic testing procedure, as described in [96], is to take the onset of this force plateau as the start for crack growth which seems to be a reasonable criterion regarding the respective SE micrographs. Yet, this onset of a constant force might depend on the sample size which would then lead to size dependent fracture toughness $K_{Iq,\delta}$. To determine the fracture toughness from the CTOD data, the value of yield strength is needed. From nanoindentation experiments Iqbal et al. [57] derived the micro-scale yield strength for NiAl and returned a value of ca. 1.8 GPa, which is slightly higher than literature data for the hard orientation, and an order of magnitude higher than reported for the soft orientation [110].

4.8.5. Overview of fracture toughness of NiAl

The fracture toughness evaluation of NiAl single crystals according to different techniques is summarized in Fig. 22 for the two orientations and two different specimen sizes. The smaller micro-cantilevers have a *H:L:W:B* dimensions of ca. 2:7:2.5:2 and the larger ones (see Fig. 20a) 4:30:9:7 (in microns). The data is compared to macroscopic fracture toughness data by Bergmann and Vehoff [104], evaluated by LEFM using large specimen sizes.

At all length scales and for all evaluation techniques, the soft orientation shows lower fracture toughness compared to the hard orientation. Because of its inherent brittleness and low amount of crack tip plasticity, the results for the soft orientation match well for the micro-scale testing techniques. Applying CTOD and LEFM techniques, a somewhat lower bound for the fracture toughness is obtained of ca. 1.9 MPa $m^{1/2}$, in good agreement with literature. *J*-Integral technique delivers a higher value with $K_{Iq} \approx 3.5$ MPa $m^{1/2}$, because *R*-curve testing could not be performed for the soft orientation due to finite crack growth prior to spontaneous failure. In this way, only the basic *J*-

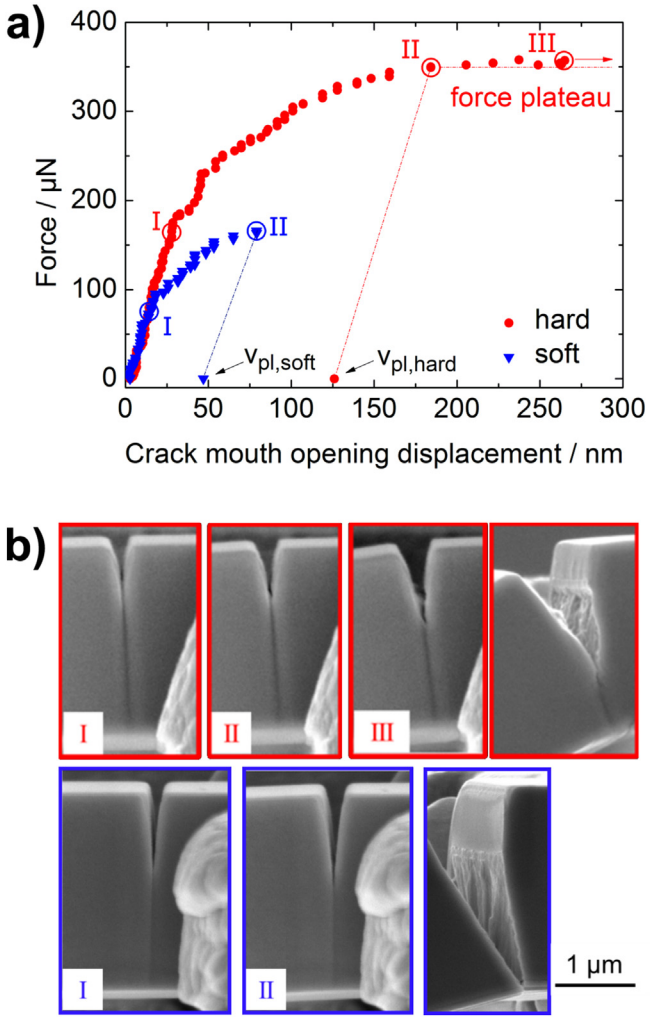

Fig. 21. (a) Force-CMOD curves for the hard and soft orientation and (b) corresponding SEM images. The soft orientation showed brittle fracture whereas a constant force plateau was obtained for the hard orientation. The begin of the force plateau (II) was taken as final data point for the determination of $v_{pl,hard}$. Note the apparent crack growth from image (II) to (III). After testing, the samples were tilted to allow for an inclined observation of the fracture surfaces. Reproduced with permission from reference [60].

Integral approach was chosen leading to a possible overestimation of the fracture toughness. The conclusion can be drawn that a lower and an upper bound of the fracture toughness were set with the presented evaluation methods in the case of the soft ⟨110⟩ orientation at the micro-scale.

For the hard orientation, it is clearly visible from Fig. 22 that LEFM strongly underestimates the fracture toughness at the micro-scale due to pronounced crack tip plasticity. Whilst in larger four-point-bend specimens, small-scale yielding (SSY) conditions are fulfilled, this does not hold true for micro-cantilevers. Applying CTOD approach and the *J*-Integral method, the calculated fracture toughness appears to be in the same range as for macroscopic specimens, i.e. 6.9 MPa $m^{1/2}$. As there is a direct physical link between CTOD and the *J*-Integral [99], it is logical that both methods lead to the same value of approximately 8 MPa $m^{1/2}$.

4.8.6. Size of the plastic zone and measurement limitations

When investigating fracture processes in confined volumes, where crack tip plasticity predominates, it is important to follow and interpret the plastic zone evolution. The basic theoretical estimate by Irwin in Eq. (16) shows the dependence on σ_y and K_I. Macroscopic yield and flow stress values are generally remarkably lower than micro- and nano-scale compression or tensile testing data [87,111]. Therefore, one may expect more ductile behaviour, because the plastic zone size scales inversely with the square of yield strength. However, fracture toughness values close to macroscopic values were measured in the case of NiAl single crystals. This is due to the size effects, which lead to an increase in yield strength and consequently a reduction in the plastic zone size [57].

In that context, the applicability of testing standards ASTM E 399 [95], ASTM E 1820 [94] and ASTM E 1290 [96] need to be addressed. They provide a rather conservative interpretation of fracture toughness evaluation using macroscopic samples, and impose many requirements for successful testing. If LEFM were to be applied, the following dimensional requirements need to be met:

$$\left\{\begin{matrix} a \\ B \\ W-a \end{matrix}\right\} \geq 2.5\left(\frac{K_{Iq}}{\sigma_y}\right)^2 \approx 25\, r_{pl,\ plane-strain} \tag{23}$$

The minimum requirements for *a*, *B* and the ligament length (*W*-*a*) are designed to ensure that the plastic zone is sufficiently small for fracture to be *K*-controlled. Supposing a fracture toughness and a yield strength as indicated in this study, the calculated dimensions for *a*, *B* and (*W*-*a*) should be approximately an order of magnitude larger than the dimensions of the NiAl micro-cantilevers shown above. If EPFM were to be applied, the restrictions become less

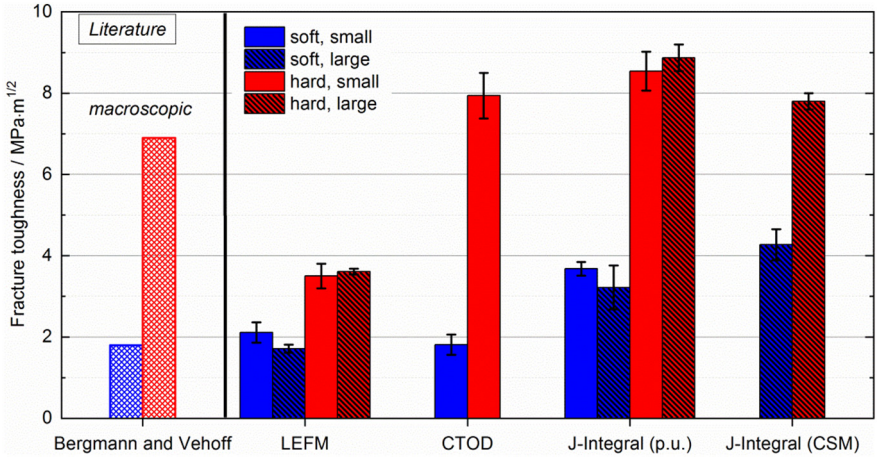

Fig. 22. Overview of fracture toughness data as evaluated by means of the different techniques; "p.u." means partial unloading; literature data taken from [104] and "small" and "large" characterise the different cantilever sizes, which were investigated in the studies presented here.

severe:

$$\left\{ \begin{matrix} B \\ W-a \end{matrix} \right\} > 10\, J_q/\sigma_y, \tag{24}$$

This shows that pronounced crack tip plasticity or large-scale yielding may lead to limitations in the interpretation of fracture toughness measurements. Applying macroscopic and microscopic yield stress data of NiAl of ca. 1.4 GPa [110] and 1.8 GPa [57], respectively, and a J_q value for the hard orientation of 200 N/m [97], characteristic lengths of 1.4 μm and 1.1 μm respectively can be calculated using Eq. (24). These lengths are just below critical cantilever dimensions and prove the validity of EPFM in the case of NiAl at the microscale. This is also the reason why the microscopic data compare well to the macroscopic data in Fig. 22. Furthermore, it is worth noting that no apparent differences were observed when testing the smaller samples under vacuum conditions and comparing their results to larger beams tested in air. However, this should not be taken as a general rule, as the outcome is likely to depend strongly on the sample size and material. For example, for W single crystals with the crack system in the ⟨100⟩{100} orientation, a strong size dependence of fracture behaviour was observed [65]. The smallest investigated cantilever size in that study with the dimensions in the submicron regime failed by brittle cleavage and displayed fracture toughness of only 1.5 MPa $m^{1/2}$, which agrees well with the Griffith theory of an ideally brittle crack. With increasing specimen size, a gradual increase in plastic deformation and hardening behaviour was noticed. Only for larger cantilever sizes with $(W\text{-}a) \geq 3$ μm, *J*-Integral evaluation led to a fracture toughness close to the macroscopic data from literature. This effect of decreasing fracture toughness with size was also found by Preiβ et al. [24] for freestanding Au films with the thicknesses of a few hundred nanometres, which exhibited brittle behaviour and a fracture toughness as low as 2 MPa $m^{1/2}$.

Finally, it should be kept in mind that the description of the plastic zone even within the framework of EPFM remains based on continuum mechanics considerations. The local stress distribution in micro-scale fracture specimens may be entirely different, also leading to a different shape of the plastic zone, as can be shown by in situ single crystal deformation mapping by HR-EBSD [67]. Studies using discrete dislocation dynamics simulations as well as advanced HR-EBSD measurements in combination with FIB-slicing approach are currently under way to elucidate the shape of the plastic zone in small-scale specimens. Also, high-resolution Digital Image Correlation (DIC) is a promising tool to understand the strain field around the crack tip in more detail. These numerical and analytical techniques in combination with micromechanical testing will be key to further successful understanding of micro-scale fracture toughness evaluation in materials showing non-negligible crack tip plasticity.

5. The influence of FIB milling on fracture toughness

FIB milling has been widely accepted as a key technique for micro- to nano-scale sample preparation, due to its nanometre precision and minimally disturbing nature. However, it may potentially induce damage in the sample by inducing ion implantation, altering surface chemistry, and modifying free volume. These effects become very important for micro-scale specimens. Numerous studies have been devoted to the assessment of sample damage due to FIB milling, e.g. [56,112–118]. In [119] it was shown for silicon that ion beam at acceleration voltages up to 30 keV affects the material to the depths of the order of 50 nm. Detailed TEM-based analysis of crack propagation through FIB-milled samples demonstrated that the artificial FIB-milled crack behaves in the manner similar to natural cracks. Ast et al. [65] demonstrated for tungsten single crystals that crack propagation was not significantly altered in the FIB-affected region. There is further evidence of rather limited material modification under the regimes relevant to micro-scale sample fabrication [120].

In order to analyze the impact of FIB damage on the fracture behaviour, Best et al. [34] carried out microscale fracture toughness tests on CrN thin films using different techniques, including single and double cantilever bending, as well as micro-pillar splitting. Fig. 23a illustrates the effect of Ga-ion milling current on fracture toughness evaluation by micro-cantilever bending. Apparent fracture toughness increased at large Ga ion currents used to fabricate the notch for crack propagation in cantilevers. The value of K_c for micro-cantilevers notched at 1 pA ion current was according to the authors close to the one determined by pillar splitting (~3.0 MPa $m^{1/2}$). They concluded from their measurements that notching with higher currents led to an increase in fracture toughness caused by penetrating Ga ions. Compared to the other applied techniques in their study, specific micro-pillar geometry enabled crack nucleation and propagation in the core of the pillar, which was minimally affected by ion damage during sample preparation, especially at large pillar diameters.

The fracture toughness trend in Fig. 23a could also be understood in the context of recent studies on the quantification of FIB-induced damage in silicon [119], in which the authors used the combination of experiments and modelling to evaluate the FIB-induced inelastic strain (eigenstrain) associated with silicon amorphisation at the periphery of the pillar. Noticeably, the induced residual strain in the pillars was found to increase with increasing FIB milling currents. Therefore, the observed effect of FIB damage on pillar splitting may be associated with residual stress field affecting the critical load for

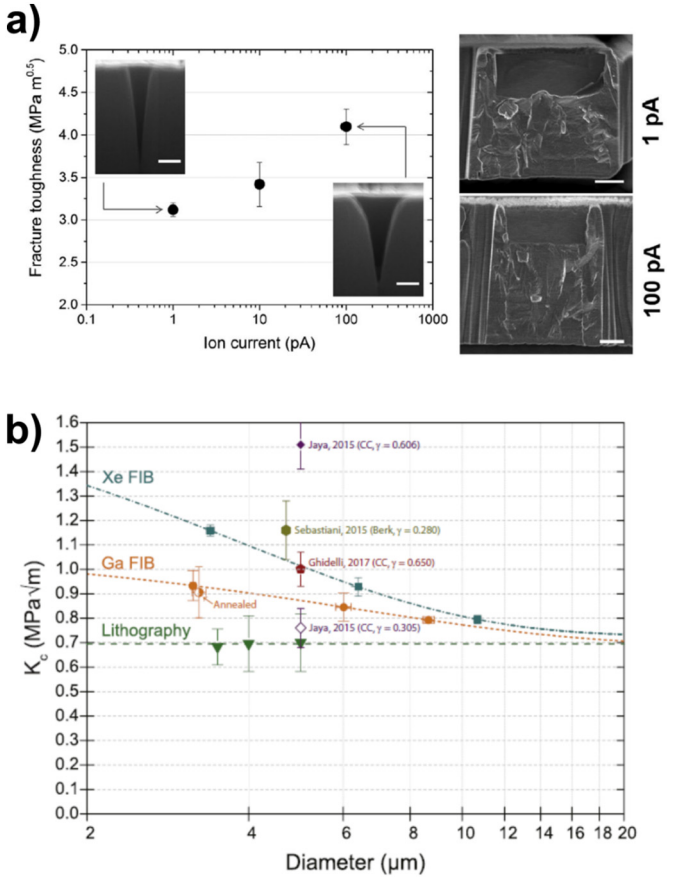

Fig. 23. a) Fracture toughness of CrN micro-cantilevers as a function of gallium ion current during notching. SEM images of FIB-polished cross sections of notches milled at 1 pA and 100 pA (inset, scale bar 100 nm), and HR-SEM images of the fractured cantilever surface post-fracture for 1 and 100 pA ion currents (scale bar 500 nm), after [34]. b) Variation of K_c as a function of pillar size for different production methods with indenter geometry (CC – cube corner, Berk – Berkovich) and γ coefficient [36]. Reproduced with permission from references [34] and [36], respectively.

crack instability, even though crack nucleation occurs in the center of the pillar.

On the other hand, it is important to consider sample preparation effects that may also influence fracture toughness evaluation. Material bridges at the two notch sides, which are meant to produce sharp starter cracks as discussed previously and as also used by Best et al. [34], and also slightly blunt crack tips [121] can lead to an overestimation of the fracture toughness. Whether toughening effects by ion-sample interaction take place, or whether notch preparation effects play an important role has to be examined in detail in specific context of experimental set-up realization and material.

A detailed study of the effect of FIB damage for the extraction of K_c in silicon by pillar splitting performed by Lauener et al. [36] was mentioned earlier. The authors investigated the variation of K_c for pillars with different diameters, milled using different ions (Xe^+, Ga^+), see Fig. 23b. A comparison with pillars prepared by photolithography (without the use of FIB) was also carried out. FIB machining was found to produce an increase in the measured toughness, especially for smaller pillars. As the pillar size was increased (>5 μm), the results from pillars prepared by FIB milling appear to converge towards the constant plateau matching the data for lithography pillars. Moreover, Fig. 23b shows that FIB milling affects mainly the external surface of the pillar, with the increase of K_c being correlated with reducing pillar diameter, and therefore a larger surface/volume ratio. This effect is more pronounced (nearly twice) for Xe ions, which are heavier, induce more damage, and have a greater effect on the crack propagation.

To sum up this section, one of the key advantages of pillar splitting is related to the more limited FIB damage (in comparison to micro-cantilever testing), which affects mainly the external surface of the pillar leading to a limited influence on the crack propagation. However, the effects from FIB-induced residual strains can be expected to be present in pillar splitting, especially for smaller diameters and those materials that show amorphisation due to FIB milling. In order to reduce ion damage of the surface, pillars should be milled using Ga ions with lowest possible current.

6. Discussion

It has become apparent from the foregoing presentation that the challenges involved in micro-scale toughness evaluation are significant, both practically, i.e. in terms of sample preparation to fabricate the required miniature test specimens, whilst avoiding artefacts associated with material modification, and correct application of load; and in terms of interpretation through simulation and analysis, given the variety of deformation modes, and the frequently encountered impossibility of ensuring compliance with existing testing standards. It is therefore worthwhile posing again the question as to the practical benefits and improved insights that are garnered that make it worthwhile.

The development of micro- and nano-technologies in the course of the last four decades brought with it the inevitable improved understanding of the deformation and failure mechanisms at these scales, and how these affect the overall structural integrity and performance of components and assemblies. Accepting this, there arises the wish to use these insights to achieve better, more efficient and reliable designs.

One area of application where the methods reviewed here make a crucial difference concerns microelectronic circuits, where the inexorable drive towards miniaturization and 3D integration brought about the use of Through Silicon Vias (TSV's) as a means of interconnecting different circuit layers [123]. Since the connecting wire (typically Cu) is different from the surrounding material (typically Si) in terms of thermal expansion coefficient, stiffness, and hardness, significant residual stresses arise during operation. These may drive the processes of crack initiation and propagation within TSV that ultimately limit the durability and performance of the assembly. Attempts to apply conventional macro-scale fracture mechanics analyses to such systems run into limitations that have already been touched upon in the above review: even if classical approaches are used for analysis (which in itself is subject to debate), key parameters describing the material resistance to crack propagation must be obtained experimentally. There is no possibility of doing it at the macroscopic scale, due to the fact that component assembly exerts pronounced effects on the structure of materials and interfaces. Therefore, micro-scale in situ testing must be used.

Another area where micro-scale toughness testing is required concerns alloys used in the fabrication of aeroengine components, such as Ti-6Al-4V. In recent years the importance of so-called “facet fatigue” phenomenon has been highlighted [124]. This concerns the initiation of cracks at grain boundaries between grains with different crystal orientation with respect to applied loading. This mode of failure is particularly important under conditions of dwell, when sustained exposure to tensile stress may lead to local strain accumulation and crack initiation. Although the ultimate aim of ensuring structural integrity of macroscopic components is being pursued, it is the micro-scale fracture processes that determine the outcome, via the principle of the “weakest link”. Here again, local fracture toughness testing offers answers that cannot be obtained otherwise.

There are many other contexts in which similar observations can be made, which explained the reasons for the growing popularity of the subject of the present review with researchers. It is clear that although conventional macro-scale methods served us well for many decades, there is an increasing realization that in many situations size effects arise that limit our ability to perform reliable re-scaling from conventional millimeter laboratory dimensions down to the micro- to nano-scale phenomena [125]. This situation is not entirely dissimilar to the challenge faced by researchers in civil engineering, where reliable prediction of the integrity of large structures needs to be made on the basis of smaller scale tests – with the distinction downscaling of testing is actually possible, as the present review amply demonstrates. The present report is aimed at helping researchers take advantage of the possibilities presented by the modern fine-scale experimental approaches, which is both necessary and exciting.

7. Conclusions

The review presented above provided a snapshot of the current landscape in the field of fracture toughness evaluation at the micro- to nano-scale. This direction of research is firmly embedded in the well-established disciplines of Linear Elastic Fracture Mechanics (LEFM) and Elastic-Plastic Fracture Mechanics (EPFM). The paradigm of hierarchically structured materials [122] postulates that physical quantities such as toughness may undergo discontinuous scaling transitions when the characteristic dimensions of consideration change in a way that invokes different fundamental physical laws describing the response of material to loading, and manifest themselves in the mode of deformation. In the case of toughness, the evaluation of this physical quantity using miniature samples of a few micrometers in size and smaller requires the fabrication of miniature specimens subjected to very low loads, resulting in the deformation response that is dominated by microstructural features such as grain boundaries, interfaces, dislocations, and other defects. As a consequence, the apparent values of toughness that are deduced from these experiments may differ from macroscopic values obtained by averaging (or, more precisely, by coarse graining) across larger volumes. The results reveal micro-scale inhomogeneity of structure and properties that have hitherto not been appreciated before, but which in turn represent a manifestation of the underlying structures that are present at even finer scale.

Two specific methods of toughness evaluation have formed the focus of the present review. These are micro-pillar splitting and micro-cantilever bending. In both cases, the fabrication of specimens is often accomplished by ion beam milling, which engenders certain properties of the samples. Namely, the inevitable implantation of ions and the accompanying ion beam modification of material structure introduces layers of altered material, which, despite being rather thin (~50 nm in thickness, as

a guide), may modify the material response compared to that of parent, or virgin material. Whilst every attempt has been made to minimize this effect, and various means of verifying the correctness of deductions about the underlying material were used, further effort is required to exclude the influence of sample preparation on the results.

The first method reviewed in the present study was the micro-pillar splitting approach. This method obviates the necessity of creating a pre-crack that is used to initiate fracture, and thus minimizes the influence of ion beam milling on the results. However, it has been shown that the method in its current form is suitable for materials that display a certain combination of strength and fracture toughness. Furthermore, the calibration of key conversion parameter γ is required for the evaluation. Nevertheless, this method has already shown its versatility and efficiency, and will undergo further development, particularly in application to coatings and spatially resolved K_{Ic} mapping studies.

Micro-cantilever bending as a means of toughness evaluation has matured into a well-established technique that allows precisely located and spatially resolved measurements able to reveal the influence of thin films, grain boundaries and other features on the local fracture toughness of material. Various mathematical representations useful in the evaluation of toughness were presented, and examples of application of this technique were given.

Reviewing the progress made since the seminal papers on fracture mechanics were published in *Materials & Design* forty years ago, it is abundantly clear that the evaluation of material resistance to fracture at the macroscopic scale has matured into a robust discipline that underpins mechanical design and structural integrity calculations in a number of important technological fields, from aerospace to power generation to chemical engineering. Fracture toughness determination and crack propagation testing procedures became codified in a number of standards that ensure reliability and repeatability of results. However, the application of these methods to micro- to nano-scale test pieces presents a number of challenges, including sample fabrication and manipulation, data interpretation, and standardization. The authors of this review are active in advancing knowledge in this field, in close collaboration with theorists and specialists in materials modelling at ever finer scales.

CRediT authorship contribution statement

J. Ast: Conceptualization, Data curation, Investigation, Methodology, Visualization, Writing - original draft. **M. Ghidelli:** Conceptualization, Data curation, Investigation, Visualization, Writing - original draft. **K. Durst:** Conceptualization, Writing - original draft. **M. Göken:** Conceptualization, Data curation, Investigation, Investigation, Methodology, Visualization, Writing - original draft. **M. Sebastiani:** Conceptualization, Data curation, Supervision, Writing - review & editing. **A.M. Korsunsky:** Conceptualization, Methodology, Data curation, Supervision, Writing - original draft.

Acknowledgement

Karsten Durst acknowledges continuous support of the German science foundation DFG via grant DU 424. Marco Sebastiani efforts received funding from the European Union, within the European H2020 project OYSTER, Grant Agreement No. 760827. Alexander M. Korsunsky acknowledges the support from EPSRC UK (grants EP/S005072/1 "Strategic Partnership in Computational Science for Advanced Simulation and Modelling of Engineering Systems - ASiMoV"; EP/P005381/1 "Tackling human dental caries by multi-modal correlative microscopy and multi-physics modelling"; EP/I020691/1 "Multi-disciplinary Centre for In-situ Processing Studies (CIPS)"; EP/H003215/1 "New Dimensions of Engineering Science at Large Facilities") and the Royal Society, UK (IEC \R2\170223), as well as Diamond Light Source, UK. FIB micro-pillar fabrication and nanoindentation splitting experiments were performed at the interdepartmental laboratory of electron microscopy (LIME) of "Roma TRE" University, Rome, Italy.

References

[1] A.A. Griffith, The phenomena of rupture and flow in solids, Philosophical Transactions of the Royal Society of London A: Mathematical, Physical and Engineering Sciences. 221 (1921) 163–198, https://doi.org/10.1098/rsta.1921.0006.
[2] C.E. Inglis, Stresses in Plates Due to the Presence of Cracks and Sharp Corners, 55, 1913 219–241.
[3] J.W. Gibbs, On the equilibrium of heterogeneous substances, Transactions of the Connecticut Academy of Arts and Sciences. 3 (1874) 108–248, 343–524. doi:DOI: 10.11588/heidok.00013220.
[4] D.A. Porter, K.E. Easterling, Phase Transformations in Metals and Alloys (Revised Reprint), CRC Press, 2009https://doi.org/10.1201/9781439883570.
[5] G.R. Irwin, Analysis of stresses and strains near the end of cracking traversing a plate, J. Appl. Mech. 24 (1957) 361–364.
[6] J.W. Hutchinson, Singular behaviour at the end of a tensile crack in a hardening material, Journal of the Mechanics and Physics of Solids. 16 (1968) 13–31, https://doi.org/10.1016/0022-5096(68)90014-8.
[7] J.R. Rice, G.F. Rosengren, Plane strain deformation near a crack tip in a power-law hardening material, Journal of the Mechanics and Physics of Solids. 16 (1968) 1–12, https://doi.org/10.1016/0022-5096(68)90013-6.
[8] B. Lawn, R. Wilshaw, Indentation fracture: principles and applications, J. Mater. Sci. 10 (1975) 1049–1081, https://doi.org/10.1007/BF00823224.
[9] A.G. Evans, E.A. Charles, Fracture toughness determinations by indentation, J. Am. Ceram. Soc. 59 (1976) 371–372, https://doi.org/10.1111/j.1151-2916.1976.tb10991.x.
[10] D.B. Marshall, B.R. Lawn, Residual stress effects in sharp contact cracking, J. Mater. Sci. 14 (1979) 2001–2012, https://doi.org/10.1007/BF00551043.
[11] B.R. Lawn, A.G. Evans, D.B. Marshall, Elastic/plastic indentation damage in ceramics: the median/radial crack system, J. Am. Ceram. Soc. 63 (1980) 574–581, https://doi.org/10.1111/j.1151-2916.1980.tb10768.x.
[12] J. Jang, G.M. Pharr, Influence of indenter angle on cracking in Si and Ge during nanoindentation, Acta Mater. 56 (2008) 4458–4469, https://doi.org/10.1016/j.actamat.2008.05.005.
[13] M.T. Laugier, Palmqvist indentation toughness in WC-Co composites, J. Mater. Sci. Lett. 6 (1987) 897–900, https://doi.org/10.1007/BF01729862.
[14] K.I. Schiffmann, Determination of fracture toughness of bulk materials and thin films by nanoindentation: comparison of different models, Philos. Mag. 91 (2011) 1163–1178, https://doi.org/10.1080/14786435.2010.487984.
[15] G.r. Anstis, P. Chantikul, B.r. Lawn, D.B. Marshall, A critical evaluation of indentation techniques for measuring fracture toughness: I, direct crack measurements, J. Am. Ceram. Soc. 64 (1981) 533–538, https://doi.org/10.1111/j.1151-2916.1981.tb10320.x.
[16] R.F. Cook, G.M. Pharr, Direct observation and analysis of indentation cracking in glasses and ceramics, J. Am. Ceram. Soc. 73 (1990) 787–817, https://doi.org/10.1111/j.1151-2916.1990.tb05119.x.
[17] J.H. Lee, Y.F. Gao, K.E. Johanns, G.M. Pharr, Cohesive interface simulations of indentation cracking as a fracture toughness measurement method for brittle materials, Acta Mater. 60 (2012) 5448–5467, https://doi.org/10.1016/j.actamat.2012.07.011.
[18] K.E. Johanns, J.H. Lee, Y.F. Gao, G.M. Pharr, An evaluation of the advantages and limitations in simulating indentation cracking with cohesive zone finite elements, Modelling Simul. Mater. Sci. Eng. 22 (2013), 015011. https://doi.org/10.1088/0965-0393/22/1/015011.
[19] S. Bruns, K.E. Johanns, H.U.R. Rehman, G.M. Pharr, K. Durst, Constitutive modeling of indentation cracking in fused silica, J. Am. Ceram. Soc. 100 (2017) 1928–1940, https://doi.org/10.1111/jace.14734.
[20] D.S. Gianola, A. Sedlmayr, R. Mönig, C.A. Volkert, R.C. Major, E. Cyrankowski, S.a.S. Asif, O.L. Warren, O. Kraft, In situ nanomechanical testing in focused ion beam and scanning electron microscopes, Rev. Sci. Instrum. 82 (2011), 063901. https://doi.org/10.1063/1.3595423.
[21] M. Legros, D.S. Gianola, C. Motz, Quantitative in situ mechanical testing in electron microscopes, MRS Bull. 35 (2010) 354–360, https://doi.org/10.1557/mrs2010.567.
[22] D. Kiener, C. Motz, G. Dehm, R. Pippan, Overview on established and novel FIB based miniaturized mechanical testing using in-situ SEM, IJMR. 100 (2009) 1074–1087, https://doi.org/10.3139/146.110149.
[23] B. Merle, M. Göken, Fracture toughness of silicon nitride thin films of different thicknesses as measured by bulge tests, Acta Mater. 59 (2011) 1772–1779, https://doi.org/10.1016/j.actamat.2010.11.043.
[24] E.I. Preiß, B. Merle, M. Göken, Understanding the extremely low fracture toughness of freestanding gold thin films by in-situ bulge testing in an AFM, Mater. Sci. Eng. A 691 (2017) 218–225, https://doi.org/10.1016/j.msea.2017.03.037.
[25] E.I. Preiß, F. Gannott, M. Göken, B. Merle, Scaling of the fracture toughness of freestanding metallic thin films with the yield strength, Materials Research Letters. 6 (2018) 607–612, https://doi.org/10.1080/21663831.2018.1520749.
[26] J.J. Schwiedrzik, J. Ast, L. Pethö, X. Maeder, J. Michler, A new push-pull sample design for microscale mode 1 fracture toughness measurements under uniaxial tension, Fatigue & Fracture of Engineering Materials & Structures 41 (2018) 991–1001, https://doi.org/10.1111/ffe.12741.
[27] B.N. Jaya, V. Jayaram, S.K. Biswas, A new method for fracture toughness determination of graded (Pt,Ni)Al bond coats by microbeam bend tests, Philos. Mag. 92 (2012) 3326–3345, https://doi.org/10.1080/14786435.2012.669068.
[28] E.D. Hintsala, S. Bhowmick, X. Yueyue, R. Ballarini, S.A.S. Asif, W.W. Gerberich, Temperature dependent fracture initiation in microscale silicon, Scr. Mater. 130 (2017) 78–82, https://doi.org/10.1016/j.scriptamat.2016.11.016.
[29] S. Liu, J.M. Wheeler, P.R. Howie, X.T. Zeng, J. Michler, W.J. Clegg, Measuring the fracture resistance of hard coatings, Appl. Phys. Lett. 102 (2013), 171907. https://doi.org/10.1063/1.4803928.

[30] G. Sernicola, T. Giovannini, P. Patel, J.R. Kermode, D.S. Balint, T.B. Britton, F. Giuliani, In situ stable crack growth at the micron scale, Nat. Commun. 8 (2017), 108. https://doi.org/10.1038/s41467-017-00139-w.

[31] M. Sebastiani, K.E. Johanns, E.G. Herbert, F. Carassiti, G.M. Pharr, A novel pillar indentation splitting test for measuring fracture toughness of thin ceramic coatings, Philos. Mag. 95 (2015) 1928–1944, https://doi.org/10.1080/14786435.2014.913110.

[32] M. Sebastiani, K.E. Johanns, E.G. Herbert, G.M. Pharr, Measurement of fracture toughness by nanoindentation methods: recent advances and future challenges, Curr. Opinion Solid State Mater. Sci. 19 (2015) 324–333, https://doi.org/10.1016/j.cossms.2015.04.003.

[33] R. Schöngrundner, R. Treml, T. Antretter, D. Kozic, W. Ecker, D. Kiener, R. Brunner, Critical assessment of the determination of residual stress profiles in thin films by means of the ion beam layer removal method, Thin Solid Films 564 (2014) 321–330, https://doi.org/10.1016/j.tsf.2014.06.003.

[34] J.P. Best, J. Zechner, J.M. Wheeler, R. Schoeppner, M. Morstein, J. Michler, Small-scale fracture toughness of ceramic thin films: the effects of specimen geometry, ion beam notching and high temperature on chromium nitride toughness evaluation, Philos. Mag. 96 (2016) 3552–3569, https://doi.org/10.1080/14786435.2016.1223891.

[35] M. Ghidelli, M. Sebastiani, K.E. Johanns, G.M. Pharr, Effects of indenter angle on micro-scale fracture toughness measurement by pillar splitting, J. Am. Ceram. Soc. 100 (2017) 5731–5738, https://doi.org/10.1111/jace.15093.

[36] C.M. Lauener, L. Petho, M. Chen, Y. Xiao, J. Michler, J.M. Wheeler, Fracture of silicon: influence of rate, positioning accuracy, FIB machining, and elevated temperatures on toughness measured by pillar indentation splitting, Mater. Des. 142 (2018) 340–349, https://doi.org/10.1016/j.matdes.2018.01.015.

[37] A.-N. Wang, J.F. Nonemacher, G. Yan, M. Finsterbusch, J. Malzbender, M. Krüger, Mechanical properties of the solid electrolyte Al-substituted Li7La3Zr2O12 (LLZO) by utilizing micro-pillar indentation splitting test, J. Eur. Ceram. Soc. 38 (2018) 3201–3209, https://doi.org/10.1016/j.jeurceramsoc.2018.02.032.

[38] M.Z. Mughal, H.-Y. Amanieu, R. Moscatelli, M. Sebastiani, A comparison of micro-scale techniques for determining fracture toughness of LiMn2O4 particles, Materials (Basel). 10 (2017)https://doi.org/10.3390/ma10040403.

[39] M.Z. Mughal, R. Moscatelli, H.-Y. Amanieu, M. Sebastiani, Effect of lithiation on micro-scale fracture toughness of LixMn2O4 cathode, Scr. Mater. 116 (2016) 62–66, https://doi.org/10.1016/j.scriptamat.2016.01.023.

[40] H.T. Liu, L.W. Yang, S. Han, H.F. Cheng, W.G. Mao, J.M. Molina-Aldareguía, Interface controlled micro- and macro- mechanical properties of aluminosilicate fiber reinforced SiC matrix composites, J. Eur. Ceram. Soc. 37 (2017) 883–890, https://doi.org/10.1016/j.jeurceramsoc.2016.10.003.

[41] G. Bolelli, M.G. Righi, M.Z. Mughal, R. Moscatelli, O. Ligabue, N. Antolotti, M. Sebastiani, L. Lusvarghi, E. Bemporad, Damage progression in thermal barrier coating systems during thermal cycling: a nano-mechanical assessment, Mater. Des. 166 (2019), 107615. https://doi.org/10.1016/j.matdes.2019.107615.

[42] J.P. Best, J. Wehrs, M. Polyakov, M. Morstein, J. Michler, High temperature fracture toughness of ceramic coatings evaluated using micro-pillar splitting, Scr. Mater. 162 (2019) 190–194, https://doi.org/10.1016/j.scriptamat.2018.11.013.

[43] D. Di Maio, S.G. Roberts, Measuring fracture toughness of coatings using focused-ion-beam-machined microbeams, J. Mater. Res. 20 (2005) 299–302, https://doi.org/10.1557/JMR.2005.0048.

[44] T.P. Halford, K. Takashima, Y. Higo, P. Bowen, Fracture tests of microsized TiAl specimens, Fatigue Fract. Eng. Mater. Struct. 28 (2005) 695–701, https://doi.org/10.1111/j.1460-2695.2005.00893.x.

[45] B.N. Jaya, C. Kirchlechner, G. Dehm, Can microscale fracture tests provide reliable fracture toughness values? A case study in silicon, J. Mater. Res. 30 (2015) 686–698, https://doi.org/10.1557/jmr.2015.2.

[46] K. Matoy, H. Schönherr, T. Detzel, T. Schöberl, R. Pippan, C. Motz, G. Dehm, A comparative micro-cantilever study of the mechanical behavior of silicon based passivation films, Thin Solid Films 518 (2009) 247–256, https://doi.org/10.1016/j.tsf.2009.07.143.

[47] M.J. Pfeifenberger, M. Mangang, S. Wurster, J. Reiser, A. Hohenwarter, W. Pfleging, D. Kiener, R. Pippan, The use of femtosecond laser ablation as a novel tool for rapid micro-mechanical sample preparation, Mater. Des. 121 (2017) 109–118, https://doi.org/10.1016/j.matdes.2017.02.012.

[48] C. Bohnert, N.J. Schmitt, S.M. Weygand, O. Kraft, R. Schwaiger, Fracture toughness characterization of single-crystalline tungsten using notched micro-cantilever specimens, Int. J. Plast. 81 (2016) 1–17.

[49] D.E.J. Armstrong, A.J. Wilkinson, S.G. Roberts, Micro-mechanical measurements of fracture toughness of bismuth embrittled copper grain boundaries, Philos. Mag. Lett. 91 (2011) 394–400, https://doi.org/10.1080/09500839.2011.573813.

[50] G. Žagar, V. Pejchal, M.G. Mueller, L. Michelet, A. Mortensen, Fracture toughness measurement in fused quartz using triangular chevron-notched micro-cantilevers, Scr. Mater. 112 (2016) 132–135, https://doi.org/10.1016/j.scriptamat.2015.09.032.

[51] S. Wurster, C. Motz, R. Pippan, Characterization of the fracture toughness of micro-sized tungsten single crystal notched specimens, Philos. Mag. 92 (2012) 1803–1825.

[52] S. Brinckmann, K. Matoy, C. Kirchlechner, G. Dehm, On the influence of microcantilever pre-crack geometries on the apparent fracture toughness of brittle materials, Acta Mater. 136 (2017) 281–287, https://doi.org/10.1016/j.actamat.2017.07.014.

[53] M.G. Mueller, V. Pejchal, G. Žagar, A. Singh, M. Cantoni, A. Mortensen, Fracture toughness testing of nanocrystalline alumina and fused quartz using chevron-notched microbeams, Acta Mater. 86 (2015) 385–395, https://doi.org/10.1016/j.actamat.2014.12.016.

[54] M.G. Mueller, G. Žagar, A. Mortensen, Stable room-temperature micron-scale crack growth in single-crystalline silicon, J. Mater. Res. 32 (2017) 3617–3626, https://doi.org/10.1557/jmr.2017.238.

[55] F.Y. Cui, R.P. Vinci, A chevron-notched bowtie micro-beam bend test for fracture toughness measurement of brittle materials, Scr. Mater. 132 (2017) 53–57, https://doi.org/10.1016/j.scriptamat.2017.01.031.

[56] J.P. Best, J. Zechner, I. Shorubalko, J.V. Oboňa, J. Wehrs, M. Morstein, J. Michler, A comparison of three different notching ions for small-scale fracture toughness measurement, Scr. Mater. 112 (2016) 71–74, https://doi.org/10.1016/j.scriptamat.2015.09.014.

[57] F. Iqbal, J. Ast, M. Göken, K. Durst, In situ micro-cantilever tests to study fracture properties of NiAl single crystals, Acta Mater. 60 (2012) 1193–1200.

[58] J. Ast, J.J. Schwiedrzik, J. Wehrs, D. Frey, M.N. Polyakov, J. Michler, X. Maeder, The brittle-ductile transition of tungsten single crystals at the micro-scale, Mater. Des. 152 (2018) 168–180, https://doi.org/10.1016/j.matdes.2018.04.009.

[59] S. Brinckmann, C. Kirchlechner, G. Dehm, Stress intensity factor dependence on anisotropy and geometry during micro-fracture experiments, Scr. Mater. 127 (2017) 76–78, https://doi.org/10.1016/j.scriptamat.2016.08.027.

[60] J. Ast, T. Przybilla, V. Maier, K. Durst, M. Göken, Microcantilever bending experiments in NiAl - evaluation, size effects, and crack tip plasticity, J. Mater. Res. 29 (2014) 2129–2140.

[61] M. Alfreider, D. Kozic, O. Kolednik, D. Kiener, In-situ elastic-plastic fracture mechanics on the microscale by means of continuous dynamical testing, Mater. Des. 148 (2018) 177–187, https://doi.org/10.1016/j.matdes.2018.03.051.

[62] C. Bohnert, S.M. Weygand, N.J. Schmitt, R. Schwaiger, O. Kraft, Orientation dependence of the fracture behavior of single-crystal tungsten, Procedia Mater. Sci. 3 (2014) 479–484, https://doi.org/10.1016/j.mspro.2014.06.080.

[63] N.J. Schmitt, C. Bohnert, C. Eberl, R. Schwaiger, S.M. Weygand, O. Kraft, Investigation of the fracture behavior of tungsten at the micro scale, 13th International Conference on Fracture, 4, 2013, pp. 3342–3349.

[64] D.E.J. Armstrong, C.D. Hardie, J.S.K.L. Gibson, A.J. Bushby, P.D. Edmondson, S.G. Roberts, Small-scale characterisation of irradiated nuclear materials: part II nanoindentation and micro-cantilever testing of ion irradiated nuclear materials, J. Nucl. Mater. 462 (2015) 374–381.

[65] J. Ast, M. Göken, K. Durst, Size-dependent fracture toughness of tungsten, Acta Mater. 138 (2017) 198–211, https://doi.org/10.1016/j.actamat.2017.07.030.

[66] J. Ast, M. N. Polyakov, G. Mohanty, J. Michler, X. Maeder, Interplay of stresses, plasticity at crack tips and small sample dimensions revealed by in-situ microcantilever tests in tungsten, Mater. Sci. Eng. A 710 (2018) 400–412, https://doi.org/10.1016/j.msea.2017.10.096.

[67] J. Ast, G. Mohanty, Y. Guo, J. Michler, X. Maeder, In situ micromechanical testing of tungsten micro-cantilevers using HR-EBSD for the assessment of deformation evolution, Mater. Des. 117 (2017) 265–266, https://doi.org/10.1016/j.matdes.2016.12.052.

[68] D. Kupka, E.T. Lilleodden, Mechanical testing of solid-solid interfaces at the micro-scale, Exp. Mech. 52 (2012) 649–658.

[69] D. Kupka, N. Huber, E.T. Lilleodden, A combined experimental-numerical approach for elasto-plastic fracture of individual grain boundaries, Journal of the Mechanics and Physics of Solids. 64 (2014) 455–467, https://doi.org/10.1016/j.jmps.2013.12.004.

[70] D.E.J. Armstrong, M.E. Rogers, S.G. Roberts, Micromechanical testing of stress corrosion cracking of individual grain boundaries, Scr. Mater. 61 (2009) 741–743, https://doi.org/10.1016/j.scriptamat.2009.06.017.

[71] H. Dugdale, D.E.J. Armstrong, E. Tarleton, S.G. Roberts, S. Lozano-Perez, How oxidized grain boundaries fail, Acta Mater. 61 (2013) 4707–4713, https://doi.org/10.1016/j.actamat.2013.05.012.

[72] R. Webler, M. Krottenthaler, S. Neumeier, K. Durst, M. Göken, Local fracture toughness and residual stress measurements on NiAl bond coats by microcantilever and FIB based bar milling tests, Superalloys 2012 2012, pp. 93–102.

[73] K. Matoy, T. Detzel, M. Müller, C. Motz, G. Dehm, Interface fracture properties of thin films studied by using the micro-cantilever deflection technique, Surf. Coat. Technol. 204 (2009) 878–881.

[74] H. Hirakata, Y. Takahashi, D.V. Truong, T. Kitamura, Role of plasticity on interface crack initiation from a free edge and propagation in a nano-component, Int. J. Fract. 145 (2007) 261–271, https://doi.org/10.1007/s10704-007-9079-0.

[75] E. Kawai, K. Sanada, T. Sumigawa, T. Kitamura, Delamination crack initiation from copper/silicon nitride interface edge with nanoscale singular stress field, Eng. Fract. Mech. 120 (2014) 60–66, https://doi.org/10.1016/j.engfracmech.2014.02.001.

[76] Y. Takahashi, S. Arai, Y. Yamamoto, K. Higuchi, H. Kondo, Y. Kitagawa, S. Muto, N. Tanaka, Evaluation of interfacial fracture strength in micro-scale components combined with high-voltage environmental Electron microscopy, Exp. Mech. 55 (2015) 1047–1056, https://doi.org/10.1007/s11340-015-0008-2.

[77] J. Schaufler, C. Schmid, K. Durst, M. Göken, Determination of the interfacial strength and fracture toughness of a-C:H coatings by in-situ microcantilever bending, Thin Solid Films 522 (2012) 480–484, https://doi.org/10.1016/j.tsf.2012.08.031.

[78] W.L. Costin, O. Lavigne, A. Kotousov, R. Ghomashchi, V. Linton, Investigation of hydrogen assisted cracking in acicular ferrite using site-specific micro-fracture tests, Mater. Sci. Eng. A 651 (2016) 859–868, https://doi.org/10.1016/j.msea.2015.11.044.

[79] Y. Deng, A. Barnoush, Hydrogen embrittlement revealed via novel in situ fracture experiments using notched micro-cantilever specimens, Acta Mater. 142 (2018) 236–247, https://doi.org/10.1016/j.actamat.2017.09.057.

[80] B.R.S. Rogne, N. Kheradmand, Y. Deng, A. Barnoush, In situ micromechanical testing in environmental scanning electron microscope: a new insight into hydrogen-assisted cracking, Acta Mater. 144 (2018) 257–268, https://doi.org/10.1016/j.actamat.2017.10.037.

[81] Y. Takahashi, H. Kondo, R. Asano, S. Arai, K. Higuchi, Y. Yamamoto, S. Muto, N. Tanaka, Direct evaluation of grain boundary hydrogen embrittlement: a micro-mechanical approach, Mater. Sci. Eng. A 661 (2016) 211–216, https://doi.org/10.1016/j.msea.2016.03.035.
[82] Y. Takahashi, I. Ashida, S. Arai, K. Higuchi, Y. Yamamoto, S. Muto, Interfacial fracture strength evaluation of Cu/SiN micro-components: applicability of the linear fracture mechanics criterion under a hydrogen environment, Int. J. Fract. 210 (2018) 223–231, https://doi.org/10.1007/s10704-018-0269-8.
[83] B.N. Jaya, J.M. Wheeler, J. Wehrs, J.P. Best, R. Soler, J. Michler, C. Kirchlechner, G. Dehm, Microscale fracture behavior of single crystal silicon beams at elevated temperatures, Nano Lett. 16 (2016) 7597–7603, https://doi.org/10.1021/acs.nanolett.6b03461.
[84] B.D. Snartland, A.B. Hagen, C. Thaulow, Fracture mechanical testing of single crystal notched α-iron micro-cantilevers, Eng. Fract. Mech. 175 (2017) 312–323, https://doi.org/10.1016/j.engfracmech.2017.01.024.
[85] G. Dehm, B.N. Jaya, R. Raghavan, C. Kirchlechner, Overview on micro- and nanomechanical testing: new insights in interface plasticity and fracture at small length scales, Acta Mater. 142 (2018) 248–282, https://doi.org/10.1016/j.actamat.2017.06.019.
[86] R. Pippan, S. Wurster, D. Kiener, Fracture mechanics of micro samples: fundamental considerations, Mater. Des. 159 (2018) 252–267, https://doi.org/10.1016/j.matdes.2018.09.004.
[87] M.D. Uchic, D.M. Dimiduk, J.N. Florando, W.D. Nix, Sample dimensions influence strength and crystal plasticity, Science. 305 (2004) 986–989.
[88] O. Kraft, P.A. Gruber, R. Mönig, D. Weygand, Plasticity in confined dimensions, Annu. Rev. Mater. Res. 40 (2010) 293–317, https://doi.org/10.1146/annurev-matsci-082908-145409.
[89] J.R. Greer, J.T.M. De Hosson, Plasticity in small-sized metallic systems: intrinsic versus extrinsic size effect, Prog. Mater. Sci. 56 (2011) 654–724, https://doi.org/10.1016/j.pmatsci.2011.01.005.
[90] C. Kirchlechner, P.J. Imrich, W. Grosinger, M.W. Kapp, J. Keckes, J.S. Micha, O. Ulrich, O. Thomas, S. Labat, C. Motz, G. Dehm, Expected and unexpected plastic behavior at the micron scale: an in situ μLaue tensile study, Acta Mater. 60 (2012) 1252–1258, https://doi.org/10.1016/j.actamat.2011.10.058.
[91] J.A. El-Awady, Unravelling the physics of size-dependent dislocation-mediated plasticity, Nat. Commun. 6 (2015), 5926. https://doi.org/10.1038/ncomms6926.
[92] S. Korte-Kerzel, Microcompression of brittle and anisotropic crystals: recent advances and current challenges in studying plasticity in hard materials, MRS Communications. 7 (2017) 109–120, https://doi.org/10.1557/mrc.2017.15.
[93] Y. Wei, J.W. Hutchinson, Steady-state crack growth and work of fracture for solids characterized by strain gradient plasticity, Journal of the Mechanics and Physics of Solids. 45 (1997) 1253–1273, https://doi.org/10.1016/S0022-5096(97)00018-5.
[94] ASTM International, ASTM E1820-13 Standard Test Method for Measurement of Fracture Toughness, West Conshohocken, PA, USA, 2013.
[95] ASTM International, ASTM E399-90 Standard Test Method for Plane-Strain Fracture Toughness of Metallic Materials, West Conshohocken, PA, USA, 1997.
[96] ASTM International, ASTM E1290-02 Standard Test Method for Crack-tip Opening Displacement (CTOD) Fracture Toughness Measurement, West Conshohocken, PA, USA, 2002.
[97] J. Ast, B. Merle, K. Durst, M. Göken, Fracture toughness evaluation of NiAl single crystals by microcantilevers—a new continuous J-integral method, J. Mater. Res. 31 (2016) 3786–3794.
[98] British Standards, BS 5762 Methods for Crack Opening Displacement (COD) Testing, London, UK, 1979.
[99] C.F. Shih, Relationships between the J-integral and the crack opening displacement for stationary and extending cracks, Journal of the Mechanics and Physics of Solids. 29 (1981) 305–326.
[100] C. Motz, T. Schöberl, R. Pippan, Mechanical properties of micro-sized copper bending beams machined by the focused ion beam technique, Acta Mater. 53 (2005) 4269–4279.
[101] C. Motz, D. Weygand, J. Senger, P. Gumbsch, Micro-bending tests: a comparison between three-dimensional discrete dislocation dynamics simulations and experiments, Acta Mater. 56 (2008) 1942–1955, https://doi.org/10.1016/j.actamat.2007.12.053.
[102] E. Demir, F. Roters, D. Raabe, Bending of single crystal microcantilever beams of cube orientation: finite element model and experiments, Journal of the Mechanics and Physics of Solids. 58 (2010) 1599–1612.
[103] K.-M. Chang, R. Darolia, H.A. Lipsitt, Cleavage fracture in B2 aluminides, Acta Metall. Mater. 40 (1992) 2727–2737.
[104] G. Bergmann, H. Vehoff, Effect of environment on the brittle-to-ductile transition of pre-cracked NiAl single and polycrystals, Mater. Sci. Eng. A 192–193 (1995) 309–315, https://doi.org/10.1016/0921-5093(95)80018-2.
[105] F. Thome, M. Göken, H. Vehoff, Study of the fracture behavior in soft and hard oriented NiAl single crystals by AFM, Proceedings of the 1998 German Symposium on Mechanical Properties of Ordered Solid Solutions, 7, 1999 491–499.
[106] R.T. Pascoe, C.W.A. Newey, Deformation modes of the intermediate phase NiAl, Phys. Status Solidi B 29 (1968) 357–366, https://doi.org/10.1002/pssb.19680290136.
[107] N. Rusović, H. Warlimont, The elastic behaviour of β2-NiAl alloys, Phys. Status Solidi A 44 (1977) 609–619, https://doi.org/10.1002/pssa.2210440225.
[108] G.C. Sih, H. Liebowitz, On the Griffith energy criterion for brittle fracture, Int. J. Solids Struct. 3 (1967) 1–22.
[109] M.H. Yoo, C.L. Fu, Cleavage fracture of ordered intermetallic alloys, Mater. Sci. Eng. A 153 (1992) 470–478, https://doi.org/10.1016/0921-5093(92)90239-W.
[110] R.D. Noebe, R.R. Bowman, M.V. Nathal, Physical and mechanical properties of the B2 compound NiAl, Int. Mater. Rev. 38 (1993) 193–232.
[111] D. Kiener, W. Grosinger, G. Dehm, R. Pippan, A further step towards an understanding of size-dependent crystal plasticity: in situ tension experiments of miniaturized single-crystal copper samples, Acta Mater. 56 (2008) 580–592, https://doi.org/10.1016/j.actamat.2007.10.015.
[112] W.J. MoberlyChan, D.P. Adams, M.J. Aziz, G. Hobler, T. Schenkel, Fundamentals of focused ion beam nanostructural processing: below, at, and above the surface, MRS Bull. 32 (2007) 424–432.
[113] D. Kiener, C. Motz, M. Rester, M. Jenko, G. Dehm, FIB damage of Cu and possible consequences for miniaturized mechanical tests, Mater. Sci. Eng. A 459 (2007) 262–272.
[114] S. Shim, H. Bei, M.K. Miller, G.M. Pharr, E.P. George, Effects of focused ion beam milling on the compressive behavior of directionally solidified micropillars and the nanoindentation response of an electropolished surface, Acta Mater. 57 (2009) 503–510, https://doi.org/10.1016/j.actamat.2008.09.033.
[115] H. Bei, S. Shim, M.K. Miller, G.M. Pharr, E.P. George, Effects of focused ion beam milling on the nanomechanical behavior of a molybdenum-alloy single crystal, Appl. Phys. Lett. 91 (2007), 111915. https://doi.org/10.1063/1.2784948.
[116] J. Guénolé, A. Prakash, E. Bitzek, Atomistic simulations of focused ion beam machining of strained silicon, Appl. Surf. Sci. 416 (2017) 86–95, https://doi.org/10.1016/j.apsusc.2017.04.027.
[117] R. Maaß, D. Grolimund, S. Van Petegem, M. Willimann, M. Jensen, H. Van Swygenhoven, T. Lehnert, M.A.M. Gijs, C.A. Volkert, E.T. Lilleodden, R. Schwaiger, Defect structure in micropillars using X-ray microdiffraction, Appl. Phys. Lett. 89 (2006), 151905. https://doi.org/10.1063/1.2358204.
[118] F. Hofmann, E. Tarleton, R.J. Harder, N.W. Phillips, P.-W. Ma, J.N. Clark, I.K. Robinson, B. Abbey, W. Liu, C.E. Beck, 3D lattice distortions and defect structures in ion-implanted nano-crystals, Sci. Rep. 7 (2017), 45993. https://doi.org/10.1038/srep45993.
[119] E. Salvati, L.R. Brandt, C. Papadaki, H. Zhang, S.M. Mousavi, D. Wermeille, A.M. Korsunsky, Nanoscale structural damage due to focused ion beam milling of silicon with Ga ions, Mater. Lett. 213 (2018) 346–349, https://doi.org/10.1016/j.matlet.2017.11.043.
[120] D. Kiener, A.M. Minor, O. Anderoglu, Y. Wang, S.A. Maloy, P. Hosemann, Application of small-scale testing for investigation of ion-beam-irradiated materials, J. Mater. Res. 27 (2) (2012) 2724–2736, https://doi.org/10.1557/jmr.2012.303.
[121] M. Creager, P.C. Paris, Elastic field equations for blunt cracks with reference to stress corrosion cracking, Int. J. Fract. 3 (1967) 247–252, https://doi.org/10.1007/BF00182890.
[122] A.M. Korsunsky, A.I. Salimon, On the paradigm of hierarchically structured materials, in conjunction with the virtual special issue on functional materials, Mater. Des. 158 (2018) 1–4, https://doi.org/10.1016/j.matdes.2018.08.008.
[123] S. Papaleo, Mechanical Reliability of Open Through Silicon Via Structures for Integrated Circuits. Ph.D. dissertation, TU Vienna (2016).
[124] F.P.E. Dunne, D. Rugg, On the mechanisms of fatigue facet nucleation in titanium alloys, Fatigue Fract. Eng. Mater. Struct. 31 (2008) 949–958.
[125] A.M. Korsunsky, Power Law Multi-scaling of Material Strength. arXiv:cond-mat/0508653 (2005).